J. Fluid Mech. (1990), *vol.* 216, *pp.* 103–132
Printed in Great Britain

Calculation of linear detonation instability: one-dimensional instability of plane detonation

By H. I. LEE AND D. S. STEWART†
Department of Theoretical and Applied Mechanics, University of Illinois, Urbana, IL 61801, USA

(Received 3 January 1989 and in revised form 12 December 1989)

The detonation stability problem is studied by a normal mode approach which greatly simplifies the calculation of linear instability of detonation in contrast to the Laplace transform procedure used by Erpenbeck. The method of solution, for an arbitrary parameter set, is a shooting method which can be automated to generate easily the required information about instability. The condition on the perturbations applied at the end of the reaction zone is shown to be interpreted as either a boundedness condition or an acoustic radiation condition. Continuous and numerically exact neutral stability curves and boundaries are given as well as growth rates and eigenfunctions which are calculated for the first time. Our calculations include the Chapman–Jouguet (CJ) case which presents no special difficulty. We give representative results for our detonation model and summarize the one-dimensional stability behaviour in parameter space. Comparison with previous results for the neutral stability boundaries and approximations to the unstable discrete spectrum are given. Parametric studies of the unstable, discrete spectrum's dependence on the activation energy and the overdrive factor are given with the implications for interpreting the physical mechanism of instability observed in experiments. This first paper is restricted to the case of one-dimensional linear instability. Extensions to transverse disturbances will be treated in a sequel.

1. Introduction

Detonation physics is a relatively new branch of combustion science that studies the mechanics and chemistry of compressible, reacting fluid flow. The detonation wave is a combustion-driven shock wave which can travel at enormous velocity (kilometres per second) and can generate enormous overpressures (tens to thousands of atmospheres). The simplest, physically relevant mathematical model of detonation is given by the reactive Euler's equations, a set of hyperbolic partial differential equations in space and time that express the conservation of mass, momentum, energy and the rate of consumption of reactant within the fluid.

Steady detonation structure is easily described, but the stability of detonations and the subsequent evolution of the instabilities are not. Detonation propagation in gas-filled tubes often exhibits a cellular, pulsating mode of propagation. The cellular propagation mode etches strikingly beautiful diamond-shaped patterns with characteristic dimensions, scribed by the triple points of the detonation shock impinging on the sidewalls of detonation tubes. Davis (Fickett & Davis 1979) has demonstrated the existence of cellular instability in a nitromethane and acetone

† Author to whom correspondence should be addressed.

condensed phase explosive. This mode of propagation is only described as an extremely nonlinear process, however the regular features of the instability are readily identifiable. A central and poorly understood problem is how the structure and linear stability characteristics of the planar detonation relate to the spacing of the nonlinear propagation. Spacing and cell size characterizations found in routine experiments are used to estimate the thermochemistry of the reaction zone (Shepherd 1986).

The linear stability problem of planar detonation requires extensive numerical treatment because the structure of the detonation wave, under sufficiently general modelling circumstances, generates ordinary differential equations with non-constant coefficients. A major goal of previous research has been to define the stability boundaries in a relevant parameter space. The most complete investigation of the neutral stability boundaries for the reactive Euler's equations is due to Erpenbeck in the 1960s at Los Alamos (Erpenbeck 1962, 1964). (A complete set of references to Erpenbeck's work is found in Fickett & Davis 1979.) In his book with Fickett, in the section on stability, Davis constructed a diagram that summarizes the totality of Erpenbeck's stability results in the appropriate parameter space: the heat of combustion, the wavenumber of disturbances transverse to the detonation shock and a chemical kinetics parameter for the chemical reaction behind the detonation shock. The diagram shown is poorly resolved and incomplete because the methods that Erpenbeck used (about which we will say more later) sampled parameter space and determined stability or instability pointwise. The stability boundaries were inferred by, sometimes, crude interpolation. It is fair to say that Erpenbeck's method is hard to implement and it does not give a computationally direct way to determine the stability boundaries or the dispersion relation that defines the unstable modes. Erpenbeck's results were largely limited to overdriven detonations because of analytical difficulties associated with the Chapman–Jouguet (CJ) detonation case.

Yet this diagram to date, has represented the best source of information about the boundaries of stability for detonation described by the reactive Euler's equations. Modern analytical studies using asymptotic methods, such as those due to Majda & Rosales (1983), Buckmaster & Ludford (1988) and Buckmaster & Nevis (1988) have been handicapped in the physical interpretations of the various modes of instability by the lack of reliable, global information on linear stability characteristics with regard to parameter space. Indeed, with the exception of Erpenbeck and the present work, there are no exact treatments of the stability problem, all other treatments have been ad hoc, asymptotic or are based on a simplified model formulation (Fickett 1985), or are without reaction zone structure.

A common assumption is that the calculation of linear stability theory, properly interpreted, will lead to prediction of the preferred cell sizes observed in the nonlinear propagation phase. Recently, new analytical theories that use asymptotics based on weak curvature of the detonation shock relative to the reaction zone thickness, have been developed by Bdzil & Stewart in a series of papers (Bdzil & Stewart 1986; Stewart & Bdzil 1988*a*, *b*). This theory is called 'Detonation Shock Dynamics' after Whitham's analogous theory for shocks and calculates multidimensional steady detonation wave propagation and temporal evolution of the near CJ detonation. In particular they show that the multi-dimensional detonation shock propagates along its normal at the CJ speed with a correction that is a function of the local total curvature of the shock. Their theory assumes that the evolutionary timescale of the main features of the detonation flow is long compared to the particle transit time

through the reaction zone. Faster evolving instabilities may disrupt this structure and the question of linear stability of the multidimensional steady or the slowly evolving detonation state is an important issue in the evaluation of the theory.

Thus the need for reliable and highly resolved information about linear stability characteristics, neutral stability boundaries, the frequencies and growth rates of unstable disturbances has directly motivated this study. This information has become extremely important for the continued advancement of nonlinear detonation theory and the evaluation of the ability of linear stability theory to predict regular patterns observed in the violent, nonlinear transverse modes and in particular in the context of modern numerical simulation and physical experiment.

In this paper we present a normal mode analysis and solve the singular eigenvalue problem by a straightforward shooting method, which in turn defines (numerically) the dispersion relation. The dispersion relation can be used to solve for the neutral stability curves directly as well as the unstable discrete spectrum. The integration of the stability ODEs gives the corresponding eigenfunctions. In §2 we give the governing equations and formulation which are consistent with Erpenbeck's. In §3 we review the steady state. In §4 we give an explicit formulation of the stability problem as a singular, eigenvalue problem with the important discussion of the condition to be applied at the end of the reaction zone which is shown to be interpreted alternatively as a boundedness or radiation condition. Importantly, we show that our formulation automatically includes the CJ case and that it presents no special difficulty. In §5 we discuss the numerical method and convergence. In §6, we give representative results for our detonation model and summarize the one-dimensional stability behaviour in parameter space. In particular we present the neutral stability boundaries and give growth rates and representative eigenfunctions. We also compare our results with all the previous analytical work on this problem that is relevant. We present parametric studies of the migration of the unstable spectrum as the activation energy and the overdrive factor is varied, and discuss the implication of our results in interpreting the physical mechanism of longitudinal instability observed in experiment. In §7, we suggest avenues for future work.

This first paper is restricted to one-dimensional disturbances evolving in the flow direction only (the wavenumber characterizing transverse disturbances is set equal to zero). Extensions to non-zero transverse wavenumbers is a straightforward extension of this work and will be treated in a sequel.

2. Formulation

The governing equations are the reactive Euler equations, which can be written in their dimensional form as

$$\frac{\mathrm{D}\rho}{\mathrm{D}t}+\rho\nabla\cdot\boldsymbol{u}'=0,\quad \frac{\mathrm{D}\boldsymbol{u}'}{\mathrm{D}t}+\rho^{-1}\nabla p=0,\quad \frac{\mathrm{D}e}{\mathrm{D}t}+p\frac{\mathrm{D}\rho^{-1}}{\mathrm{D}t}=0,$$

$$\frac{\mathrm{D}\lambda}{\mathrm{D}t}=r,\quad \frac{\mathrm{D}(\,)}{\mathrm{D}t}\equiv\frac{\partial}{\partial t}+\boldsymbol{u}'\cdot\nabla(\,)', \tag{2.1a–d}$$

where the variables ρ, $\boldsymbol{u}'$, p and λ are the density, lab frame particle velocity, pressure and reaction progress variable. Note that $\nu\equiv\rho^{-1}$ is used to identify the specific volume. The equation of state and the rate law (i.e. the specification of $e(p,\nu,\lambda)$ and $r(p,\nu,\lambda)$) characterize the explosive. For purposes of comparison and simplicity we

assume the polytropic equation of state, Arrhenius, simple-depletion form of the reaction rate and an ideal thermal equation of state,

$$e \equiv pv\frac{1}{(\gamma-1)} - Q\lambda, \quad r \equiv k(1-\lambda)\,\mathrm{e}^{(-E/R_g T)}, \quad R_g T = pv. \tag{2.2}$$

The shock relations are given generally by

$$\left.\begin{aligned} &\rho(\boldsymbol{D}'-\boldsymbol{u}')\cdot\boldsymbol{n}|_s = \rho(\boldsymbol{D}'-\boldsymbol{u}')\cdot\boldsymbol{n}|_o = m, \quad p_s - p_o = m^2(v_o - v_s), \\ &e_s - e_o = \tfrac{1}{2}(p_s+p_o)(v_o-v_s), \quad \boldsymbol{u}'\cdot\boldsymbol{l}_1|_s = \boldsymbol{u}'\cdot\boldsymbol{l}_1|_o, \quad \lambda_s = 0, \end{aligned}\right\} \tag{2.3}$$

where the o subscript refers to the state immediately ahead of the detonation shock with the s subscript used for behind the shock. The variable $\boldsymbol{D}'$, is the normal detonation shock velocity as seen in the lab frame, $\boldsymbol{n}$ is the unit normal vector to the detonation shock and $\boldsymbol{l}_i$ are the corresponding unit tangent vectors. The above formulation is the well-known multidimensional ZND detonation model. We next discuss our choice of dimensional scales and specialize to one dimension.

Dimensional scales are chosen in reference to the one-dimensional, steady detonation wave. In particular the density, pressure and velocity scales are the detonation shock density, pressure and sound speed, ρ_s, p_s, c_s. The characteristic lengthscale l_c is chosen as the steady half-reaction zone length and the characteristic timescale is the half-reaction zone length divided by the shock sound speed, l_c/c_s. From now on we will adopt the notation of a tilde ($\sim$) superscript to denote dimensional quantities and an asterisk (*) to denote the one-dimensional steady state and an ∞ subscript or superscript to denote the state at the end of the reaction zone.

3. The one-dimensional steady state

The steady one-dimensional detonation is assumed to travel to the left in the negative x-direction. The steady detonation structure is found quite simply by two steps. The first is algebraic and assumes the conservation of mass, momentum and energy at each point in the detonation wave structure (i.e. partially reacted, with $0 < \lambda < 1$, the one-dimensional, steady, Rankine–Hugoniot (R–H) relations are solved analytically). Thus if u^* is the relative, dimensionless, steady one-dimensional velocity in the wave frame and p^* and v^* are the corresponding pressure and specific volume, then from the algebra of the R–H relations we find in terms of λ^* that

$$p^* = a + (1-a)(1-b\beta\lambda^*)^{\frac{1}{2}}, \quad u^* = \frac{(1-p^*)}{(\gamma M_s)} + M_s, \quad v^* = \frac{u^*}{M_s}, \tag{3.1}$$

where M_s is the steady shock Mach number (as seen by an observer in the frame immediately behind the shock) and a and b are constants and D is the steady, dimensionless detonation velocity (whose absolute value is the Mach number of the detonation shock relative to the unshocked quiescent explosive) and β the dimensionless heat release. These quantities as well as the intermediate constants a and b are defined by the relations

$$\left.\begin{aligned} &M_s \equiv (\tilde{u}^{l*} - \tilde{D}^*)/\tilde{c}_s^*, \quad D \equiv \tilde{D}^*/\tilde{c}_o^*, \text{ with } M_s^2 = \frac{(\gamma-1)\,D^2+2}{2\gamma D^2-(\gamma-1)}, \\ &\beta \equiv \tilde{Q}\gamma/(\tilde{c}_s^*)^2, \quad a = \frac{\gamma D^2+1}{2\gamma D^2-(\gamma-1)} = \frac{\gamma M_s^2+1}{(\gamma+1)} < 1, \quad \text{since } M_s < 1, \\ &b = \frac{M_s^2\,2\gamma(\gamma-1)}{(1-a)^2(\gamma+1)}. \end{aligned}\right\} \tag{3.2}$$

Note that the steady state variables satisfy the shock conditions

$$\nu^* = P^* = 1, \quad u^* = M_s, \quad \lambda^* = 0, \quad \text{at } x = 0. \tag{3.3}$$

The steady wave is such that $D < 0$ and the structure lies such that $x > 0$.

The second step involves the integration of the one-dimensional steady rate equation to determine λ^* as a function of the wave coordinate x. Note that formulae (3.1) and the (dimensional) steady rate equation inferred from (2.1d) determine the characteristic dimensional half-reaction zone length as

$$\tilde{l}_c = \int_0^{\frac{1}{2}} [(\tilde{u}'(\lambda)^* - \tilde{D}^*)/\tilde{r}^*(\lambda)]\,\mathrm{d}\lambda = \tilde{c}_s^*\,\tilde{k}^{-1} \int_0^{\frac{1}{2}} u^*(\lambda)(1-\lambda)^{-1} \exp[\theta/(p^*\nu^*)]\,\mathrm{d}\lambda. \tag{3.4}$$

The distribution of the reaction is then governed by the integral

$$x = \int_0^{\lambda} u^*(\lambda)/r^*(\lambda)\,\mathrm{d}\lambda,$$

where

$$r^* = k(1-\lambda^*)\exp[-\theta/(p^*\nu^*)], \quad k = [\tilde{k}\tilde{l}_c/\tilde{c}_s^*], \quad \theta \equiv \tilde{E}/(\tilde{R}_g \tilde{T}_s^*). \tag{3.5}$$

4. The linear stability problem (formulation in the wave coordinate)

We now derive the linear stability problem. First we transform the one-dimensional governing equations to the shock attached coordinates

$$x = x' - (\tilde{D}^*/\tilde{c}_s^*)\,t - \psi(t), t, \tag{4.1}$$

where u is now the particle velocity relative to the steady frame

$$u = u' - (\tilde{D}^*/\tilde{c}_s^*). \tag{4.2}$$

The governing system of equations (mass, momentum, energy and rate) are simply represented in matrix form as

$$\boldsymbol{z}_{,t} + \boldsymbol{A} \cdot \boldsymbol{z}_{,x} - \boldsymbol{b}\psi_{,t} = \boldsymbol{c}, \tag{4.3}$$

where

$$\boldsymbol{z} = \begin{bmatrix} \nu \\ u \\ p \\ \lambda \end{bmatrix}, \quad \boldsymbol{A} = \begin{bmatrix} u & -\nu & 0 & 0 \\ 0 & u & \nu/\gamma & 0 \\ 0 & \gamma p & u & 0 \\ 0 & 0 & 0 & u \end{bmatrix}, \quad \boldsymbol{b} = \begin{bmatrix} \nu_{,x} \\ u_{,x} \\ p_{,x} \\ \lambda_{,x} \end{bmatrix}, \quad \boldsymbol{c} = \begin{bmatrix} 0 \\ 0 \\ (\gamma-1)\beta r/\nu \\ r \end{bmatrix}. \tag{4.4}$$

We linearize the above equations and seek solutions to a normal mode expansion of the form

$$\boldsymbol{z} = \boldsymbol{z}^*(x) + \boldsymbol{z}'(x)\exp(\alpha t), \quad \psi = \psi' \exp(\alpha t), \tag{4.5}$$

where the prime superscript refers to a small perturbation. For complex α, $\boldsymbol{z}'$ is complex, likewise ψ' is a complex scalar. The linearized perturbation equations reduce directly to

$$\alpha \boldsymbol{z}' + \boldsymbol{A}^* \cdot \boldsymbol{z}'_{,x} + \boldsymbol{C}^* \cdot \boldsymbol{z}' - \alpha \boldsymbol{b}^* \psi' = 0. \tag{4.6}$$

The definition of $\boldsymbol{A}^*$ and $\boldsymbol{b}^*$ follow directly from (4.4), whereas $\boldsymbol{C}^*$ is a matrix defined by the steady state which has contributions from both $\boldsymbol{A} \cdot \boldsymbol{z}_{,x}$ and $\boldsymbol{c}$ in (4.3) namely

$$\boldsymbol{C}^* = \begin{bmatrix} -u_{,x} & \nu_{,x} & 0 & 0 \\ p_{,x}/\gamma & u_{,x} & 0 & 0 \\ -\dfrac{(\gamma-1)\beta}{\nu}[r_{,\nu} - r/\nu] & p_{,x} & \gamma u_{,x} - \dfrac{(\gamma-1)\beta}{\nu} r_{,p} & -\dfrac{(\gamma-1)\beta}{\nu} r_{,\lambda} \\ -r_{,\nu} & \lambda_{,x} & -r_{,p} & -r_{,\lambda} \end{bmatrix}^*, \tag{4.7}$$

where the sensitivities of the reaction rate r with respect to the thermodynamic variables corresponding to (2.2) are given explicitly by

$$r_{,\nu} = \frac{r\theta}{(\nu T)}, \quad r_{,p} = \frac{r\theta}{(pT)}, \quad r_{,\lambda} = -k\exp\left(\frac{-\theta}{T}\right) < 0. \tag{4.8}$$

The perturbed shock conditions derive boundary conditions for (4.6). The perturbed shock conditions are arrived at by the following steps. First, (2.3) are specialized to the unsteady shock attached frame using the definitions of (4.1) and (4.2) to determine the normal detonation velocity, $\tilde{D}_n = \tilde{D} + \tilde{\psi}_{,t}$. These relations are then linearized according to the normal mode expansion (4.5) finally obtaining

$$\nu' = \frac{4}{(\gamma+1)D^2M_s}\alpha\psi', \quad u' = \frac{2(D^2+1)}{(\gamma+1)D^2}\alpha\psi', \quad p' = -\frac{4\gamma M_s}{(\gamma+1)}\alpha\psi', \quad \lambda' = 0. \tag{4.9}$$

4.1. *The linear stability problem (formulation in the reaction coordinate)*

For a single reaction rate with a monotone decreasing reactant with distance in the reaction zone, we can replace the wave coordinate with the reaction coordinate. In particular, we introduce the independent variable $s \equiv \lambda^*(x)$ such that

$$\partial/\partial x = (r^*/u^*)\,\partial/\partial s, \tag{4.10}$$

and in particular the derivatives in the definition of $\boldsymbol{C}^*$ and $\boldsymbol{b}^*$ are modified according to definitions (4.7) and (4.4c) respectively. For convenience we normalize the perturbation z' with respect to its shock value (4.9) by defining

$$\boldsymbol{\zeta} = \boldsymbol{S}^{-1}\cdot \boldsymbol{z}'/\psi', \tag{4.11}$$

where

$$\boldsymbol{S} = \begin{bmatrix} \dfrac{4}{(\gamma+1)D^2M_s} & 0 & 0 & 0 \\ 0 & \dfrac{2(D^2+1)}{(\gamma+1)D^2} & 0 & 0 \\ 0 & 0 & -\dfrac{4\gamma M_s}{(\gamma+1)} & 0 \\ 0 & 0 & 0 & 1 \end{bmatrix}. \tag{4.12}$$

Using the change of variable (4.10) and definition (4.11) in (4.6), followed by solving for $\mathrm{d}\boldsymbol{\zeta}/\mathrm{d}s$, we obtain

$$\mathrm{d}\boldsymbol{\zeta}/\mathrm{d}s = -\alpha\boldsymbol{F}^*\cdot\boldsymbol{\zeta} - \boldsymbol{G}^*\cdot\boldsymbol{\zeta} + \alpha\boldsymbol{h}^*, \tag{4.13}$$

where the steady state matrices $\boldsymbol{F}^*$, $\boldsymbol{G}^*$ and $\boldsymbol{h}^*$ are real functions of the steady reaction coordinate s defined by

$$\boldsymbol{F}^* = \left(\frac{u^*}{r^*}\right)\boldsymbol{S}^{-1}\cdot\boldsymbol{A}^{*-1}\cdot\boldsymbol{S}, \quad \boldsymbol{G}^* = \left(\frac{u^*}{r^*}\right)\boldsymbol{S}^{-1}\cdot\boldsymbol{A}^{*-1}\cdot\boldsymbol{C}^*\cdot\boldsymbol{S}, \quad \boldsymbol{h}^* = \left(\frac{u^*}{r^*}\right)\boldsymbol{S}^{-1}\cdot\boldsymbol{A}^{*-1}\cdot\boldsymbol{b}^*. \tag{4.14}$$

The shock conditions become initial values (at $s = 0$) that are needed to solve the ODEs in the reaction coordinate. Because of our normalization of the perturbations, these become simply

$$\boldsymbol{\zeta}(0) = \alpha\boldsymbol{d}, \quad \boldsymbol{d} = (1,1,1,0). \tag{4.15}$$

For a given value of α, a solution to the stability equations is defined by integration to the end of the reaction zone ($s = 1, r^* = 0$). However, in order to

determine the dispersion relation (derived by the normal mode expansion) an additional condition which is discussed next, must be given. We show in the next section that this condition is a boundedness condition of perturbations at the end of the reaction zone and is equivalent to a 'radiation' condition, i.e. that no waves emanate from the equilibrium zone to interfere with the evolution of the perturbed solution.

4.2. *Discussion of the rear boundary condition*

In order to solve the initial-value problem of unsteady detonation propagation, it is common to prescribe a condition at some distance behind the detonation shock. This condition is called the 'piston condition' and the material velocity is prescribed to be exactly the velocity of a supporting piston at the piston location. The piston is usually placed at the end of the reaction zone in the following flow.

When models of steady detonation are considered, the length of the reaction zone is calculated from the resolved rate law. The length of the zone corresponding to complete reaction, calculated in terms of half-reaction lengths, can be inferred from (3.5) to be

$$l_{rz} = \int_0^1 u^*(\lambda)/r^*(\lambda)\,\mathrm{d}\lambda. \tag{4.16}$$

It can be clearly seen from (4.16) that the steady reaction zone length is finite or infinite if the above integral is convergent or divergent which, in turn, depends on the functional form of $r^*(\lambda)$. Since we concentrate on the rates with simple depletion (i.e. $r^* \sim (1-\lambda)$ as did Erpenbeck and most other researchers), the steady reaction zone length is infinite.

Thus any condition that we place on the stability perturbations at the end of the reaction zone is applied at an infinite distance as measured from the detonation shock. Because of the weak logarithmic singularity of (4.16), a practical infinity may only be a few half reaction zone thicknesses from the detonation shock. Our conclusions about the character of the stability of our flow depend on the assumption of simple depletion in the sense that we must apply a condition on the solution at a boundary at an infinite distance from the shock instead of a finite distance from the shock. The stability of detonation flows corresponding to reaction rates that produce finite length reaction zones must be studied separately, but probably can be studied by the methodology given here.

A simplifying assumption that has been made in prior research on the stability problem, is to assume that perturbations in the rear of the flow that propagate forward to interfere with the detonation shock, can have no causal influence on the stability since such disturbances would take an infinite time to disturb the entire detonation flow. Thus a more natural boundary condition, that of a constant velocity piston at infinity (say) is replaced by a statement that no acoustic waves on forward characteristics emanate from the piston to influence the detonation. This condition has been labelled a 'causality' condition in Buckmaster & Ludford (1988) and we use the terminology 'radiation' condition which is common to acoustics.

Regardless of the view that is taken on how to model the flow at the end of the reaction zone, one additional, homogeneous, boundary condition is required in order to close the system of equations to derive the dispersion relation. Subsequently we will derive this condition in two distinct ways and in each case, the condition is the same. The first, physically based, derivation of the 'radiation' condition is an acoustic analysis of the flow near the end of the reaction zone. The second derivation is based on the requirement that only spatially bounded solutions to the stability perturbations equations are allowed when considering unstable modes. The explicit

condition we derive in this way is essentially the boundedness condition applied by Erpenbeck in his Laplace-transform based formulation of this problem. We give both derivations and show that they are equivalent in order to clarify the physical and mathematical interpretation of the 'radiation condition' as applied to these spatially unbounded detonation flows.

We point out that the choice of the homogeneous condition, consistent with a given flow, determines in part the final stability results. For example, one can still imagine applying a condition other than the radiation condition. For the constant velocity piston, the perturbation particle velocity at the unperturbed piston location is zero. Other types of rear support conditions can be considered as well, corresponding to slightly different idealizations or different physical experiments. Different support conditions will ultimately lead to different stability conclusions. However the methodology presented here is expected to work well for other cases and the constant velocity piston condition has been tested by us and is discussed briefly in §6.4.

4.2.1. *Acoustics at the end of the reaction zone*

At the end of the reaction zone the detonation state is near its complete reacted, equilibrium value. Thus we can assume that the solution may be represented as its R–H, equilibrium value plus an acoustic perturbation. In terms of z, x and t this expansion would be represented as

$$z = z_\infty + z'(x,t), \quad z' \sim z^{\mathrm{a}}, \tag{4.17}$$

where the ∞ subscript refers to the reacted equilibrium state of the steady detonation and the 'a' superscript refers to an 'acoustic' expansion. The expansions inserted in the governing equations generate a set of linear, constant coefficient, hyperbolic partial differential equations in x and t,

$$z^{\mathrm{a}}_{,t} + \boldsymbol{A}^\infty \cdot z^{\mathrm{a}}_{,x} = \boldsymbol{c}^\infty \lambda^{\mathrm{a}}, \tag{4.18}$$

where $\boldsymbol{A}^\infty$ follows directly from (4.4b) and $\boldsymbol{c}^\infty$ is given by

$$\boldsymbol{c}^\infty = r^\infty_{,\lambda} \begin{bmatrix} 0 \\ 0 \\ (\gamma-1)\beta/\nu_\infty \\ 1 \end{bmatrix}. \tag{4.19}$$

The general solution is derived as follows. First the solution for λ^{a} is found directly and can be written as

$$\lambda^{\mathrm{a}} \equiv (\boldsymbol{r}_4)_4 = \exp[r^\infty_{,\lambda} t] F_4(x - u_\infty t), \tag{4.20}$$

and for the purposes of the acoustic analysis we can assume the arbitrary F_4 to be a single Fourier component. Thus we carry out the solution with

$$F_4 = \exp[(r^\infty_{,\lambda}/c_\infty) k(x - u_\infty t)], \quad \text{where } k \text{ is complex.} \tag{4.21}$$

Then by direct substitution it is simple to verify that the general solution can be written as

$$z^{\mathrm{a}} = F_1(x-u_\infty t)\,\boldsymbol{r}_1 + F_2(x-(u_\infty+c_\infty)t)\,\boldsymbol{r}_2 + F_3(x-(u_\infty-c_\infty)t)\,\boldsymbol{r}_3 + \boldsymbol{r}_4 \exp\{(r^\infty_{,\lambda}/c_\infty)[k(x-u_\infty t)+c_\infty t]\}, \tag{4.22}$$

where

$$\left.\begin{aligned} \boldsymbol{r}_1^{\mathrm{T}} &= (1,0,0,0), \quad \boldsymbol{r}_2^{\mathrm{T}} = (-\nu_\infty, c_\infty, \gamma p_\infty, 0), \quad \boldsymbol{r}_3^{\mathrm{T}} = (-\nu_\infty, -c_\infty, \gamma p_\infty, 0) \\ \boldsymbol{r}_4^{\mathrm{T}} &= (-k_1 k^2 \nu_\infty, -k_1 k c_\infty, k_1 \gamma p_\infty, 1), \quad k_1 = (\gamma-1)\beta/[(1-k^2)\gamma p_\infty \nu_\infty]. \end{aligned}\right\} \tag{4.23}$$

In (4.22), $F_i \boldsymbol{r}_i$, $i = 1, 2, 3$, correspond to the travelling-wave solutions of the homogeneous, inert acoustics problem around the equilibrium state. The last independent solution, $\boldsymbol{r}_4$ can be found by solving for a particular solution to the first three acoustic equations of (4.18), with λ^{a} known.

The radiation condition requires that there be no perturbation to the steady state at the end of the reaction zone that travels towards the shock from the piston. This requirement sets $F_3 = 0$. Then, if the disturbance is to be represented by three linearly independent solutions to the acoustic equations instead of four, an algebraic constraint on the solution must be satisfied which is homogeneous. In particular from (4.22) we see that u^{a}, p^{a}, λ^{a} must be expressed as a linear combination of F_2 and $\exp\{(r_{,\lambda}^{\infty}/c_\infty)[k(x-u_\infty t)+c_\infty t]\}$. The necessary constraint relating u^{a}, p^{a}, λ^{a} is that

$$[(\gamma-1)\beta/(\gamma c_\infty^2)]\lambda^{\mathrm{a}} + (1-k)[u^{\mathrm{a}}/c_\infty - p^{\mathrm{a}}/(\gamma p_\infty)] = 0. \tag{4.24}$$

Finally, we convert this acoustic wave result to the nomenclature of our stability formulation in the wave coordinate x. In particular, this conversion identifies k in terms of the growth rate α. For example, the function $\exp\{(r_{,\lambda}^{\infty}/c_\infty)[k(x-u_\infty t)+c_\infty t]\}$, appearing in our acoustic solution at the end of the reaction zone can be written as $f(x)\exp(\alpha t)$, thus identifying

$$\alpha = r_{,\lambda}^{\infty}(1-ku_\infty/c_\infty). \tag{4.25}$$

Equation (4.24) rewritten in terms of α (with $\boldsymbol{z}^{\mathrm{a}} \sim \boldsymbol{z}'$) obtains

$$-[(\gamma^2-1)\beta u_\infty/(\gamma c_\infty^3)]\lambda' + [(1-u_\infty/c_\infty) - \alpha/r_{,\lambda}^{\infty}](u'/c_\infty - p'/(\gamma p_\infty)) = 0. \tag{4.26}$$

Rewriting (4.26) in terms of ζ, $M_\infty \equiv u_\infty/c_\infty$ and D (for the implementation of the shooting method) shows

$$\begin{aligned} H(\alpha) &= -(\gamma^2-1)\beta/[4\gamma c_\infty] M_\infty \zeta_4 + [(1-M_\infty) - \alpha/r_{,\lambda}^{\infty}][(D^2+1)/(2D^2)\zeta_2 + M_\infty \zeta_3] = 0, \\ &\equiv H(\alpha;\gamma,\beta,\theta,D) = 0. \end{aligned} \tag{4.27}$$

To our knowledge condition (4.26)–(4.27) has not appeared in this explicit form before. In the asymptotic studies of Buckmaster & Ludford (1988) and in the structureless analysis of Majda & Rosales (1983) the condition that appears sets $\lambda' = 0$, and does not account for the perturbation of the reaction rate in the equilibrium region. Also, in Erpenbeck's work and the approximate analysis given by Abouseif & Toong (1982), this condition is implied but never explicitly written. It is also important to note that the radiation condition is not singular for the CJ limit where $M_\infty = 1$. Indeed, the previous acoustic analysis applies equally well to the case of overdriven and CJ detonation waves.

4.2.2. *The boundedness condition at the end of the reaction zone*

Now we explore the structure of the solutions of the perturbation equations near the equilibrium point and we show that we derive exactly condition (4.26)–(4.27) as the boundedness condition at the end of the reaction zone. First, we notice that the steady state perturbation equations, in the reaction coordinate s are singular at the *end* of the reaction zone, $r^* \to 0$ as $s \to 1$. For both the overdriven and the CJ detonations, one source of singularity is the vanishing of the steady reaction term as $r^* \to 0$. For the CJ detonations, an additional singularity arises through the fact that

the steady flow is sonic at the end of the reaction zone. The sonic parameter is defined by

$$\eta \equiv 1-M^2, \quad M^2 = u^2/c^2, \tag{4.28}$$

and $\eta_{\mathrm{CJ}} \to 0$ as $s \to 1$.

To show this more clearly, the asymptotic behaviour of $\boldsymbol{F}^*$, $\boldsymbol{G}^*$ and $\boldsymbol{h}^*$ in (4.14) can be found directly from their definitions as

$$\boldsymbol{F}^* \sim O(1/(\eta r^*)), \quad \boldsymbol{G}^* \sim O(1/(\eta(1-s))), \quad \boldsymbol{h}^* \sim O(1/\eta), \tag{4.29}$$

where the general dependence on the form of the depletion factor depends on the detailed specification of r^*. For simple depletion the rate is proportional to $(1-s)$. The sonic parameter η vanishes at the end of the reaction zone only for the CJ case when it has the asymptotic behaviour

$$\eta_{\mathrm{CJ}} \sim (1-s)^{\frac{1}{2}}(1-M_{\mathrm{s}}^2)/a, \tag{4.30}$$

where a is defined in (3.2*d*).

The sonic parameter, η, appears through the dependence of $\boldsymbol{F}^*$, $\boldsymbol{G}^*$ and $\boldsymbol{h}^*$ on $\boldsymbol{A}^{*-1}$ which is given by

$$\boldsymbol{A}^{*-1} = \eta^{-1}\begin{bmatrix} \eta/u & -\nu/c^2 & \nu^2/(\gamma u c^2) & 0 \\ 0 & -u/c^2 & \nu/(\gamma c^2) & 0 \\ 0 & \gamma p/c^2 & -u/c^2 & 0 \\ 0 & 0 & 0 & \eta/u \end{bmatrix}^*. \tag{4.31}$$

The explicit appearance of the term $(1-s)$ in the asymptotic description of G^* arises from the term $r^*_{,\lambda}/r^*$ in its definition. Thus this dependence will be maintained for reactant depletion with an arbitrary power of $(1-\lambda)$.

For the overdriven case, η does not vanish as $s \to 1$ and for the case of simple depletion where $r^* \sim (1-s)$, the asymptotic form of the governing equations for the perturbations at the end of the reaction zone are given by

$$(1-s)\,\mathrm{d}\boldsymbol{\zeta}/\mathrm{d}s = -(\alpha\hat{\boldsymbol{F}}^* + \hat{\boldsymbol{G}}^*)\cdot\boldsymbol{\zeta}, \tag{4.32}$$

where

$$\hat{\boldsymbol{F}}^* = \lim_{s\to 1}(1-s)\,\boldsymbol{F}^*, \quad \hat{\boldsymbol{G}}^* = \lim_{s\to 1}(1-s)\,\boldsymbol{G}^*, \tag{4.33}$$

are constant matrices defined by the above limits.

Similarly we write down governing equations near the end of the reaction zone for the CJ case noting (4.30) to obtain

$$(1-s)^{\frac{3}{2}}\,\mathrm{d}\boldsymbol{\zeta}/\mathrm{d}s = -(\alpha\hat{\boldsymbol{F}}^*_{\mathrm{CJ}} + \hat{\boldsymbol{G}}^*_{\mathrm{CJ}})\cdot\boldsymbol{\zeta}, \tag{4.34}$$

where

$$\hat{\boldsymbol{F}}^*_{\mathrm{CJ}} = \lim_{s\to 1}(1-s)^{\frac{3}{2}}\boldsymbol{F}^*_{\mathrm{CJ}}, \quad \hat{\boldsymbol{G}}_{\mathrm{CJ}} = \lim_{s\to 1}(1-s)^{\frac{3}{2}}\hat{\boldsymbol{G}}^*_{\mathrm{CJ}}, \tag{4.35}$$

are constant matrices defined by the above limits.

In both instances, the problem of finding a solution to $\boldsymbol{\zeta}$ is simplified by introducing simple coordinate changes y, y_{CJ},

$$\left.\begin{aligned} &(1-s)^{-1}\,\mathrm{d}s = \mathrm{d}y, && \text{for overdriven detonation,} \\ &(1-s)^{-\frac{3}{2}}\,\mathrm{d}s = \mathrm{d}y_{\mathrm{CJ}}, && \text{for CJ,} \end{aligned}\right\} \tag{4.36}$$

which reduce the local governing equations to that of linear equations with constant coefficients

$$\left.\begin{aligned} &\mathrm{d}\boldsymbol{\zeta}/\mathrm{d}y = \boldsymbol{L}\cdot\boldsymbol{\zeta}, && \text{for overdriven,} \\ &\mathrm{d}\boldsymbol{\zeta}/\mathrm{d}y_{\mathrm{CJ}} = \boldsymbol{L}_{\mathrm{CJ}}\cdot\boldsymbol{\zeta} && \text{for CJ,} \end{aligned}\right\} \tag{4.37}$$

where

$$\boldsymbol{L} \equiv -(\alpha \hat{\boldsymbol{F}}^* + \hat{\boldsymbol{G}}^*), \quad \boldsymbol{L}_{\mathrm{CJ}} \equiv -(\alpha \hat{\boldsymbol{F}}^*_{\mathrm{CJ}} + \hat{\boldsymbol{G}}^*_{\mathrm{CJ}}). \tag{4.38}$$

The exact definitions of $\boldsymbol{L}$ and $\boldsymbol{L}_{\mathrm{CJ}}$ appear in Appendix A.

For both cases, the general solution has the asymptotic form

$$\zeta \sim \sum_{i=1}^{4} \boldsymbol{g}_i \exp[\mu_i y], \tag{4.39}$$

where the eigenvalues μ_i and eigenvectors $\boldsymbol{g}_i$ are found by solving the respective eigenvalue problems defined by the solutions to (4.37). Positive values of μ_i correspond to unbounded growth at the end of the reaction zone since the definitions (4.36) imply $y \sim [(-r^{\infty}_{,\lambda})/u_{\infty}]x, y_{\mathrm{CJ}} \sim 2\exp\{\tfrac{1}{2}[(-r^{\infty}_{,\lambda})/u_{\infty}]x\}$, so that $y, y_{\mathrm{CJ}} \to \infty$ as $s \to 1$. The eigenvalues μ_i are obtained as

$$\left.\begin{aligned} &\mu_1 = (\alpha/r^{\infty}_{,\lambda}), \quad \mu_2 = (\alpha/r^{\infty}_{,\lambda})M_{\infty}(1-M_{\infty})/\eta_{\infty}, \quad \mu_3 = -(\alpha/r^{\infty}_{,\lambda})M_{\infty}(1+M_{\infty})/\eta_{\infty}, \\ &\qquad\qquad \mu_4 = (a/r^{\infty}_{,\lambda}) - 1, \quad \text{for the overdriven case,} \\ &\mu_1 = 0, \quad \mu_2 = 0, \quad \mu_3 = -2(\alpha/r^{\infty}_{,\lambda})\,a/(1-M_s^2), \quad \mu_4 = 0, \\ &\qquad\qquad \text{for the CJ case.} \end{aligned}\right\} \tag{4.40}$$

The eigenvectors are found to be given simply by

$$\boldsymbol{g}_i = \boldsymbol{S}^{-1} \cdot \boldsymbol{r}_i \quad (i = 1,2,3,4), \quad \text{with } k \equiv (1-\alpha/r^{\infty}_{,\lambda})/M_{\infty}. \tag{4.41}$$

When the real part of the growth rate α is positive, corresponding to unstable perturbations, the spatially unbounded solutions correspond to the eigenvalue (vector) μ_3, since $r^{\infty}_{,\lambda} < 0$. Applying a boundedness condition requires that the asymptotic structure of the solutions for the perturbation be independent of the unbounded solution. Once again we suppress this solution and the solution vector for the perturbation must be represented by three linearly independent solutions proportional to $\boldsymbol{r}_1$, $\boldsymbol{r}_2$ and $\boldsymbol{r}_4$ and as a consequence, a homogeneous constraint is required. The relation so derived is exactly (4.26)–(4.27).

5. Discussion of the numerical solution and technique

The problem that must be solved to determine the dispersion relation is a two-point boundary-value problem which is succinctly stated in terms of complex ζ and α as

$$\mathrm{d}\zeta/\mathrm{d}s = -\alpha \boldsymbol{F}^* \cdot \zeta - \boldsymbol{G}^* \cdot \zeta + \alpha \boldsymbol{h}^* \quad \text{for } 0 \leqslant s < 1, \tag{5.1}$$

with the shock boundary condition given by

$$\zeta = \alpha \boldsymbol{d}, \quad \boldsymbol{d} \equiv (1,1,1,0) \quad \text{at the shock at } s = 0, \tag{5.2}$$

and

$$H(\alpha) = -(\gamma^2-1)\beta/[4\gamma c_{\infty}]M_{\infty}\zeta_4 + [(1-M_{\infty}) - \alpha/r^{\infty}_{,\lambda}][(D^2+1)/(2D^2)\zeta_2 + M_{\infty}\zeta_3] = 0. \tag{5.3}$$

Since α and ζ are complex, the problem consists of eight ordinary differential equations subject to eight shock and two boundary conditions in the equilibrium zone. The two extra conditions for the shooting problem can be thought of as determining α. While the problem is formulated in a general fashion, suitable for either analytic or numerical means, numerical solution provides the means for the

most comprehensive exploration of the dependence of instability on the various parameters that define the steady state. However, this last statement is true in practice only if a reasonably efficient and numerically robust algorithm is found to solve the above problem.

In order to solve this problem numerically, we adopted a shooting method. For our calculations a total of N space nodes have been used to define a uniform grid on the interval $s \in [0, 1-1/N]$. Thus as N is increased, larger physical domains are considered. First, the steady solution is developed on the grid for a set of chosen steady state parameters. This simply involves evaluation of (3.1) for p^*, u^* and ν^* with $\lambda^* = s$ and further evaluation of $\boldsymbol{F}^*$, $\boldsymbol{G}^*$ and $\boldsymbol{h}^*$ in (5.1) on the grid. Next a trial value of α is assumed and the differential equations (5.1) are integrated forward from $s = 0$ towards $s = 1$. When the numerical integration reaches $s = 1-1/N$ (say), the real and imaginary part of the function $H(\alpha)$, defined by (5.3) are evaluated.

For fixed steady state parameters, an arbitrary value of $\alpha = \alpha_r + i\alpha_i$ does not satisfy the radiation condition, $H(\alpha) = H_r + iH_i = 0$. Thus α is varied until this condition is met. A simple way to search numerically for approximations to α is to use the numerical integration to determine values of residual functions $H_r(\alpha_r, \alpha_i)$, $H_i(\alpha_r, \alpha_i)$ at the approximate end of the interval, $s = 1-1/N$ and to determine α_r, α_i as the roots which set these residuals equal to zero. An elementary, two-variable, Newton–Raphson technique was employed to provide an iterative scheme to search for the roots of the residuals and determine the eigenvalues. However, we have also searched directly for α in the complex plane by merely recording the values of the residuals as α_r and α_i are varied and then using a contour plotting routine to determine the approximate locations of zeros in the complex α-plane. We have dubbed this simple approximate method the 'carpet search'. The first method (Newton–Raphson) accurately determines a single converged eigenvalue and eigenfunction. The 'carpet search' method can readily identify multiple eigenvalues with positive real part for a given steady parameter set.

The numerical shooting method combined with the Newton–Raphson iterations on the residuals of $H(\alpha)$ has the advantage that it can be automated to search for (in principle) any two independent parameters. As a simple and important example of this, we found the neutral stability curves by setting $\alpha_r \equiv 0$ and iterating on α_i and one additional parameter. In studies that follow, this other parameter has been the overdrive factor $f \equiv (D/D_{CJ})^2$, the polytropic exponent γ, and the heat release parameter β and the dimensionless activation energy θ. In a typical numerical study, one sets all the parameters equal to their fixed values with the exception of a single pair of parameters of interest. For example, in a neutral stability study we set $\alpha_r = 0$ and all of the other parameters fixed except the heat release parameter β and searched for (α_i, β) pairs. Once a converged pair was found, it served as a seed value to iterate for other parameter pairs in that neighbourhood of parameter space. By simply using the last converged pair as a seed, we were able to calculate an entire neutral stability curve in one computer run by choosing fixed values of parameters, including f (say), iterating on (α_i, β), followed by incrementing the value of f in an outside loop. In all of our work to date, this method has worked reliably with only a few iterations (typically 6 or less) required for each convergence. A relative convergence criteria based on the residuals was chosen. The integration of the differential equations is performed by an explicit, fourth-order Runge–Kutta method with Gill's coefficients. The Jacobians of the 2×2 matrix necessary for the Newton–Raphson method are evaluated via finite differences. If modest resolution of

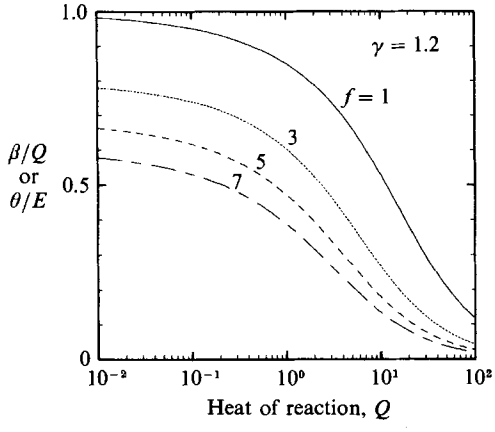

FIGURE 1. Ratios of θ/E and β/Q versus Q for varying f.

the ODEs is allowed, this method is not particularly computationally intensive and gives qualitatively accurate results.

To compare with other researcher's results, slightly different scales are introduced. The scaled activation energy and the heat release with respect to reference values in the unshocked state are defined by

$$E \equiv \tilde{E}/(\tilde{R}_g \tilde{T}_0^*), \quad Q \equiv \tilde{Q}/(\tilde{R}_g \tilde{T}_0^*), \tag{5.4}$$

whereas our corresponding parameters θ and β are scaled with respect to shock values. Our scaling has the advantage of being the natural one to discuss solutions to the differential equations behind the shock. However θ and β then depend on the shock strength or equivalently the piston velocity of a given experiment. Erpenbeck's original scaling has the advantage that E and Q are only dependent on the material properties. The relations between E and θ and between Q and β are found explicitly to be

$$\beta/Q = \theta/E \equiv [(\gamma+1)a-1][a+(a-1)q]^{-1}[\gamma a-(a-1)q]^{-1},$$

where

$$q^2 \equiv 1-[2(\gamma^2-1)QD^2]/[\gamma(D^2-1)^2]. \tag{5.5}$$

Note that $q = 0$ in (5.5) defines D_{CJ}. Equivalently, the ratios β/Q and θ/E can be written explicitly in terms of the overdrive factor $f = (D/D_{CJ}(\gamma, Q))^2$. Plots of these ratios are shown in figure 1 for varying f.

In implementing the scheme numerically, we found it convenient to solve for $(-\alpha/r_{,\lambda}^{\infty})$ so as to eliminate strong dependence of the rate on the state which occurs, in particular, for larger activation energies. An example of a convergence test of the scheme described above is shown in figure 2. The convergent eigenvalues $((-\alpha_r/r_{,\lambda}^{\infty}), (-\alpha_i/r_{,\lambda}^{\infty}))$ are plotted against the number (N) of uniform space nodes used in the integration of the stability ODEs. Usually no more than 200 space nodes were ever required to ensure convergence of the iteration and no more than 2000 nodes was required to ensure an accurate result. However, in general, the required number of nodes does depend on the parameter set under investigation. More space nodes are required (when using a uniform mesh) for the CJ case due to the stronger character of the singularity near $s = 1$ and more iteration is required. Frequent checks were made of the approximate eigenfunctions to ensure that the solutions to the perturbations equations were being numerically resolved.

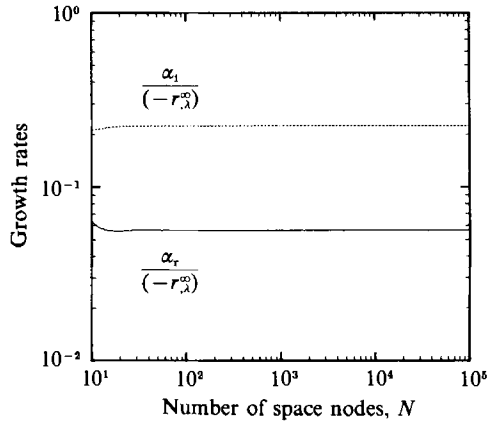

FIGURE 2. Shown is the convergence of $(-\alpha_r/r_{,\lambda}^{\infty})$, $(-\alpha_i/r_{,\lambda}^{\infty})$ found by the shooting method as the number of uniformly distributed space nodes for integration, N was increased. $\gamma = 1.2$, $E = 50$, $Q = 50$ and $f = 1.2$.

We also made a more detailed convergence test for the case of neutral stability when it was suggested that convergence based on the mesh size may be slowed (Erpenbeck & Bdzil, private communication). For some different, representative cases, where qualitative checks showed the slowest convergence, we found the order of convergence. The values of both f and $\alpha_i/(-r_{,\lambda}^{\infty})$ were fit to the formula,

$$\phi - \phi_0 = A(1/N)^B, \tag{5.6}$$

where ϕ_0, A and B were found by the fit. B determines the order of convergence. We found that for $\gamma = 1.2$, $Q = 50$, $E = 50$ that $B = 1.065$ and for $\gamma = 1.2$, $Q = 10$, $E = 50$, $B = 0.954$. These results show that for finite $(1/N)$, the critical values of f and α_i are overpredicted.

Eigenvalues with negative real part, while not applicable to conclusions about instability according to this analysis, were found owing to the fact that the condition (4.26)–(4.27) was actually applied at a finite value of $s - 1 = 1/N$. This condition can be interpreted as a physical condition, admitting negative eigenvalues which corresponds to applying the radiation condition at a large but finite distance behind the detonation shock.

Figures 3(*a*)–3(*d*) show some representative profiles of detonation structure corresponding to different parameters and their stability. Higher and lower activation energy causes the induction zone to lengthen and shorten respectively. In particular it is possible to study the important case of large activation energy by these methods, in which case the detonation reaction zone takes on the 'square wave' structure with the reactionless induction zone followed by a rapid 'fire' region and a final inert relaxation zone to the equilibrium state. Figure 4 shows the structure of a typical eigenfunction obtained.

Two-dimensional contour plots (corresponding to the carpet search), based on the residual functions of $H(\alpha)$ were made to verify the existence of multiple unstable roots and to ensure that we could identify the eigenvalue with the largest real positive part as the parameters were changed. As a consequence, we have been able to identify all of the unstable modes for a given parameter set defined by the dispersion relation, $H(\alpha; \gamma, E, Q, f) = 0$ in a given segment of the complex α-plane. A typical contour plot of a residual function is shown in figure 5, for an overdriven

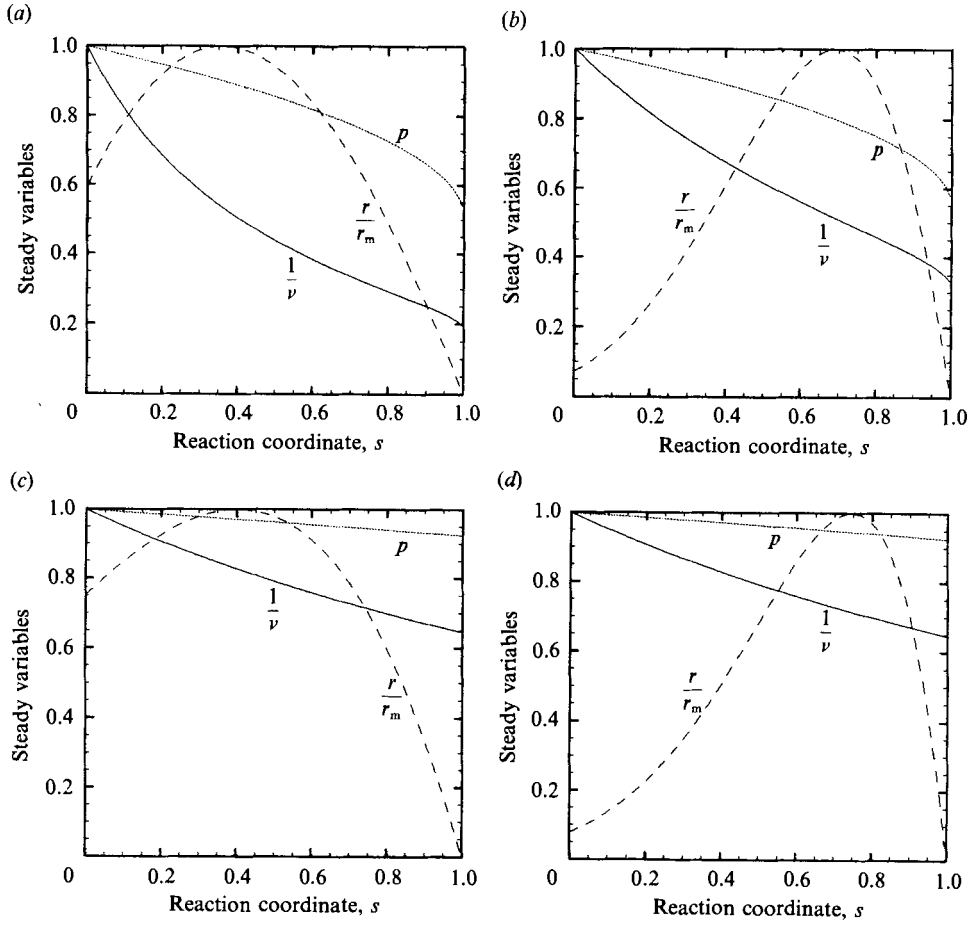

FIGURE 3. (*a*) Profiles of steady state variables displayed in the reaction coordinate, s, for the parameter set, $\gamma = 1.2$, $E = 20$, $Q = 100$, $f = 1$, (CJ). The reaction rate is normalized by its maximum value. The maximum reaction rate occurs near $s = 0.35$. This steady state is stable. (*b*) Profiles of steady state variables displayed in the reaction coordinate, s, for the parameter set, $\gamma = 1.2$, $E = 20$, $Q = 10$, $f = 1$, (CJ). The reaction rate is normalized by its maximum value. The maximum reaction rate occurs near $s = 0.70$. This steady state is unstable. (*c*) Profiles of steady state variables displayed in the reaction coordinate, s, for the parameter set, $\gamma = 1.2$, $E = 20$, $Q = 10$, $f = 3$, (overdriven). The reaction rate is normalized by its maximum value. The maximum reaction rate occurs near $s = 0.40$. This steady state is stable. (*d*) Profiles of steady state variables displayed in the reaction coordinate, s, for the parameter set, $\gamma = 1.2$, $E = 60$, $Q = 10$, $f = 3$, (overdriven). The reaction rate is normalized by its maximum value. The maximum reaction rate occurs near $s = 0.75$. This steady state is unstable.

detonation ($\gamma = 1.2, E = 50, Q = 50, f = 1.2, N = 2000$). Figure 5(*a*) shows a contour plot of a subset of the total region that we studied. The contours are the level curves of a function based on the residuals of $H(\alpha)$ given by $|H(\alpha)|^n/|\alpha/(r_\lambda^\infty)|^m$, where the constant $n = 1.2$ and $m = 1.4$ were chosen for the purpose of displaying the character of $|H(\alpha)|$. Four zero locations are shown by the contour map. Figure 5(*b*) shows a three-dimensional plot corresponding to the contour plot of figure 5(*a*) with $n = 1.2$ and $m = 1.4$. The roots are found at the local minimum points of $|H(\alpha)|$. In our studies we found that the converged root identified by the Newton–Raphson scheme depended on the starting point. The mountainous ridges identified in figure 5(*b*)

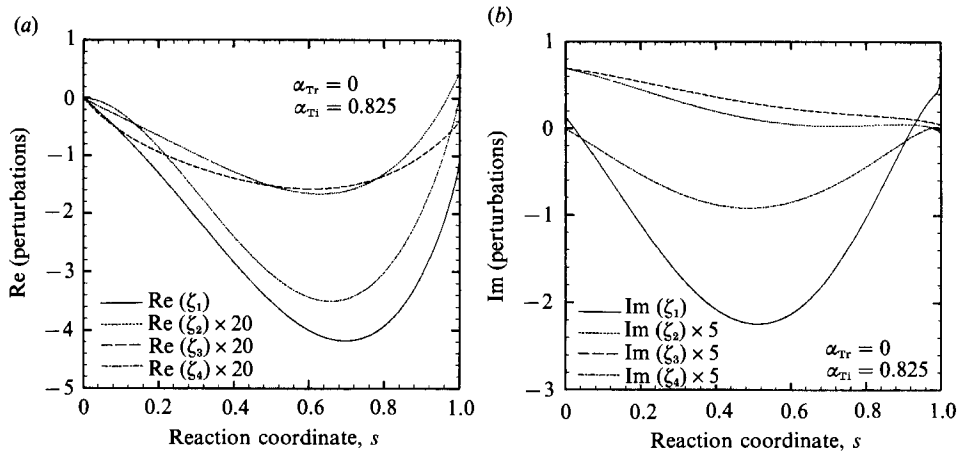

FIGURE 4. (*a*, *b*) Profiles of the real and imaginary parts of the perturbations at conditions of neutral stability. $\gamma = 1.2$, $E = 50$, $Q = 50$, $f = 1.731$. The components ζ have been scaled with respect to $(-r_{,\lambda}^{\infty})$ and the scaling factor shown.

clearly illustrate that the different roots of the dispersion relation have well-defined domains of attraction when iterative schemes such as Newton–Raphson are used to find them.

6. Discussion of results

In this section we discuss some of the results that we have obtained by this exact numerical treatment. In particular, we make comparisons of our results for neutral stability and with the unstable spectrum approximately calculated by other researchers. We also give the implications of our results in identifying the physical mechanism of longitudinal detonation instability.

6.1. *Brief history*

To elucidate our own contributions, a brief, selected history of this problem is required. More comprehensive histories can be found in chapter 6 of Fickett & Davis (1979) and in the excellent introduction found in Abouseif & Toong (1982).

The model equations used here and by other workers are found in Erpenbeck's 1962 paper on stability. Erpenbeck used the Laplace transform in time to analyse the solutions to the linearized initial-value problem and his is the only other exact treatment of plane instability, thus his results provide a basis for comparison. However, owing to the nature of his formulation and numerical method (discussed later) his results are largely confined to determining the limits of stability, and except for a very few cases, unstable growth rates and frequencies were not calculated. Also the neutral stability curves were interpolated and the continuous dependence of stability on the parameters of the system was not found.

In 1966 and 1970, the results of a nonlinear, numerical, one-dimensional simulation were published by Fickett & Wood and Fickett, Jacobson & Wood and isolated comparison of the low-frequency oscillations in the simulations were made with those calculated by Erpenbeck. In 1971 and 1972, McVey & Toong, and Alpert & Toong published studies of the detonation instability observed when blunt projectiles are fired at high speed into detonable gases. There, they elaborated a wave-interaction

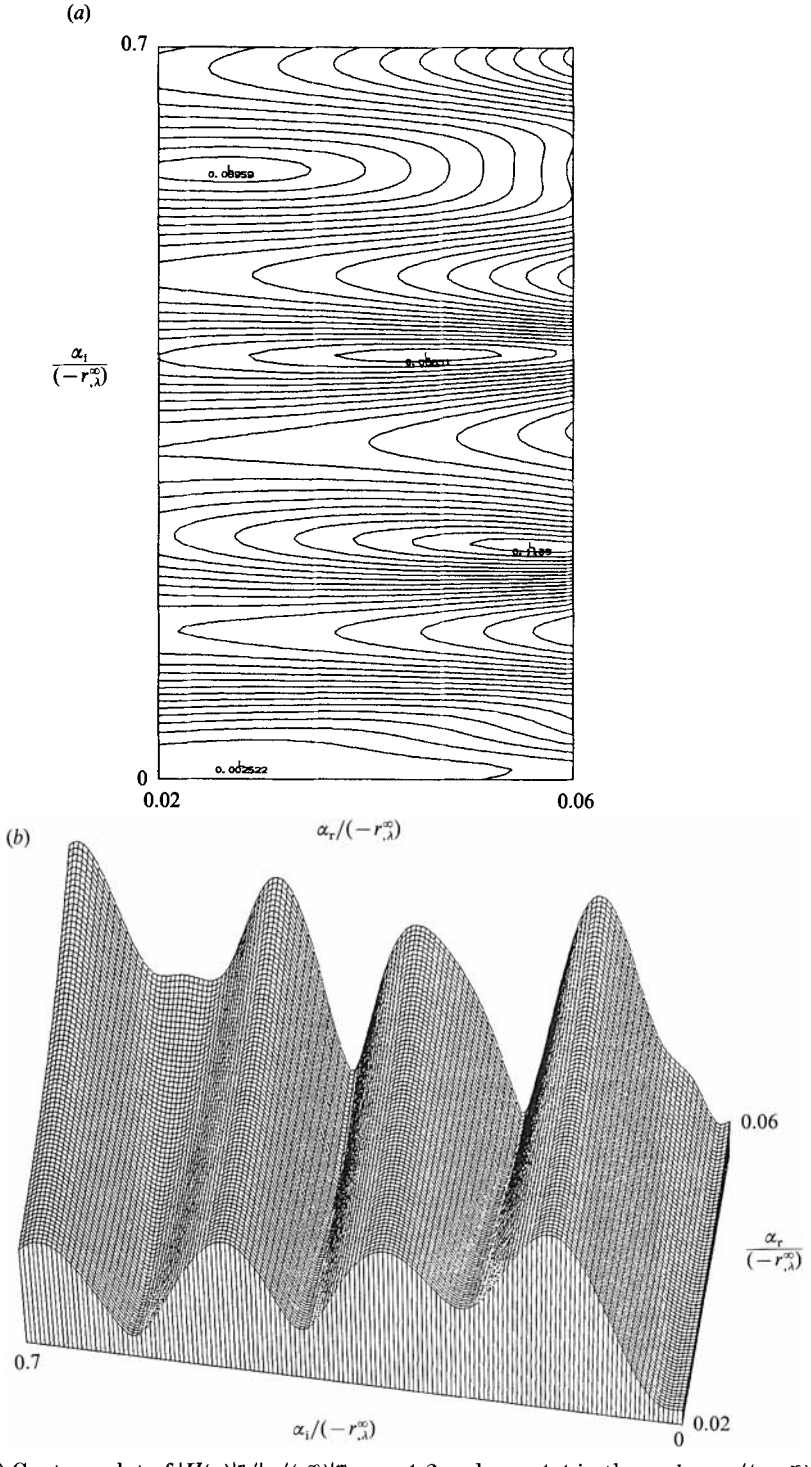

FIGURE 5. (*a*) Contour plot of $|H(\alpha)|^n/|\alpha/(r_{,\lambda}^{\infty})|^m$, $n = 1.2$ and $m = 1.4$ in the region $\alpha_r/(-r_{,\lambda}^{\infty}) \in [0.02, 0.06]$ and $\alpha_i/(-r_{,\lambda}^{\infty}) \in [0, 0.7]$. $E = 50$, $Q = 50$, $f = 1.2$, $(-r_{,\lambda}^{\infty}) = 7.926$, $N = 2000$. Four roots are located. (*b*) Three-dimensional plot of $|H(\alpha)|^n/|\alpha/(r_{,\lambda}^{\infty})|^m$, $n = 1.2$ and $m = 1.4$ in the region $\alpha_r/(-r_{,\lambda}^{\infty}) \in [0.02, 0.06]$ and $\alpha_i/(-r_{,\lambda}^{\infty}) \in [0, 0.7]$. $E = 50$, $Q = 50$, $f = 1.2$, $N = 2000$. The roots are located in the local minimums.

mechanism to describe the observed longitudinal instability which relies on the existence of an induction zone behind the lead shock. The essential ingredient of this proposed mechanism is that temperature perturbations created by acoustic disturbances reflecting off the shock and the reaction zone, change the induction time and cause the dramatic movement of the reaction zone forwards and backwards relative to the shock. From the experiments they were able to show that the periods of the oscillations were nearly proportional to the chemical induction time in hydrocarbon–air and hydrogen–oxygen mixtures.

In an attempt to theoretically predict and confirm the wave-interaction mechanism suggested earlier, Abouseif & Toong (1982) gave an approximate linear stability analysis for the normal mode instabilities with ad hoc approximations justified by arguments of large activation energy reactions, but not made by systematic asymptotic approximations. In 1988, Buckmaster & Ludford gave an asymptotic treatment of the square wave detonation for large activation energy for very low frequencies on the scale of the inverse induction time, which included the effect of transverse wave numbers. Later in 1988, Buckmaster & Nevis gave a one-dimensional stability analysis for higher frequencies on the scale of the inverse induction time, which is an attempt to carry out rigorously the asymptotic analysis of the square wave detonation first indicated by Erpenbeck (1963). Their calculation *only* considers the induction zone.

6.2. *Summary of neutral stability and comparison with Erpenbeck's results*

Erpenbeck's formulation of stability is the most general, in that solution of the initial-value problem by the Laplace transform in time contains a superposition of all the spectral modes and in particular those basis functions that can be obtained by separation of variable (normal modes). In 1962 he solved for the transform of the shock perturbation $\psi'(t)$ and the condition for instability is based on analysing the singularities of the transform function, identified by the zeros of the denominator.

Instead of devising a procedure to solve directly for these zeros, which would yield the unstable, discrete spectrum with the determination of the neutral stability curves as a special case, he used the Nyquist criteria to count the number (if any) of unstable poles of the transform of ψ' in the right half (unstable) portion of the complex plane. Erpenbeck's method requires the evaluation of the denominator of the transform function over a large semi-circular contour in the right half-plane utilizing the principle of the argument to determine the number of zeros. The definition of how the transform function varies over this contour, requires solutions to the stability equations for each point to be evaluated on the contour. Erpenbeck showed that in order to guarantee proper convergence of the result, it is necessary to discard one unbounded solution. This requirement results in a condition placed on his stability formulation that is equivalent to our condition (4.26)–(4.27) and derives from similar logic to that found in §4.2.2. The method that Erpenbeck (1964) outlined to count the number of poles is a hybrid, numerical-asymptotic scheme since the number of zeros is calculated as the sum of an asymptotically calculated contribution on the infinite semi-circular contour and a numerically evaluated contribution from a Bromwich contour line. Error estimates of his numerical method based on his published work are difficult to make as information about the mesh sizes, tolerance and convergence tests was never given.

We now turn to a discussion of our results. Figures 6, 7 and 8 show the neutral stability curves and boundaries. A neutral stability curve is determined by first setting $\alpha_r = 0$ and by solving for α_i and f (say) with the other parameters (E, Q, γ)

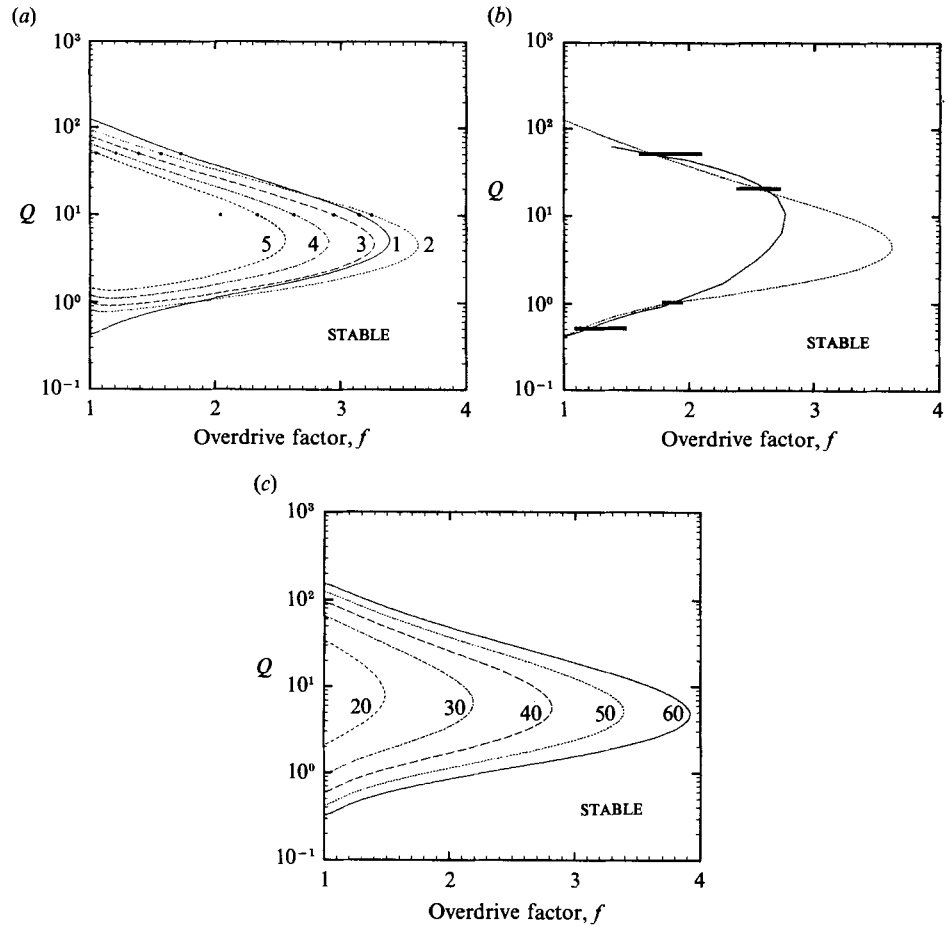

FIGURE 6. (*a*) The neutral stability curves in an (f, Q)-plane for $\gamma = 1.2$ and $E = 50$. The curves are numbered according to increasing frequency. At $Q = 10$ and 50, locations of additional neutrally stable roots are shown. (*b*) The neutral stability curve is shown as the outermost boundary of (*a*). No unstable roots are found to the right of the curve. The ends of the error bar shown indicate the points at which Erpenbeck found instability (to the left) or stability (to the right). The solid line is a reproduction of his hand-drawn interpolation. ——, Erpenbeck; ....., Lee & Stewart. (*c*) The neutral stability curves in an (f, Q)-plane for the lowest frequency (fundamental) mode for $\gamma = 1.2$ and E varying. The region to the far right is stable.

fixed. Then the curve is mapped out by slightly incrementing a second parameter Q (say) and solving for a new (f, α_i) pair. A neutral stability boundary is the curve in parameter space that defines the regions when there is, or is not, an unstable spectrum. The neutral stability boundary is in general found from a union of neutral stability curves for which the mode of neutral stability is the most unstable (rightmost). Suppose we order the unstable modes with increasing frequency, then if it were the case that the lowest frequency (fundamental) mode was always the rightmost mode, then the neutral stability boundary would be the neutral stability curve for that mode. However, this is not generally the case as the rightmost modes switch as the parameters are varied, in which case the neutral stability boundary is found by a union of segments of neutral stability curves as explained above.

Figure 6 (*a*) shows a number of neutral stability curves in a (f, Q) parameter plane for $E = 50$, $\gamma = 1.2$. Each curve shown is the result of continuous computational

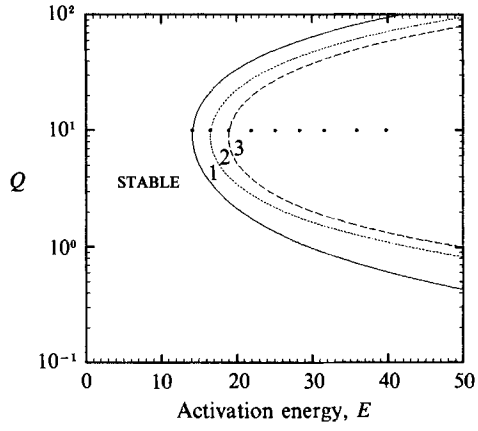

FIGURE 7. The neutral stability curves numbered by frequency for CJ detonations, shown in an (E, Q)-plane, for fixed $\gamma = 1.2$, $f = 1$. The lowest frequency neutral stability curve is the neutral stability boundary. Below a value of approximately $E = 14$ the detonations are stable.

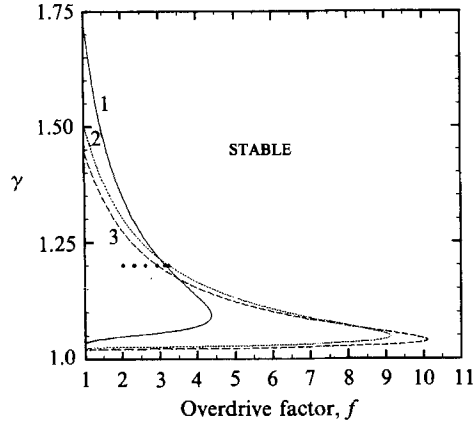

FIGURE 8. The neutral stability curves ordered by frequency in a (f, γ)-plane, for $Q = 10$ and $E = 50$. The region above and to the right of the curves shows no instability.

runs, advancing through values of the heat release Q or f. Each curve tracks a mode corresponding to its ordered frequency in the spectrum, which are numbered in the figure. The results show (for these parameter values) that the neutral stability boundary is comprised of the neutral stability curves for the first and second modes. The neutral stability curves for higher frequencies generally lie in the interior of the unstable region of the neutral stability boundary. The figure also demonstrates that logic of finding the neutral stability boundary is complicated by the fact that the most unstable modes switch to different frequencies so that many, if not all of the neutral stability curves need to be found to define the neutral stability boundary unambiguously. In this sense Erpenbeck's method for determining the neutral stability boundary, could be considered more direct. Figure 6(a) also shows the location of neutral stability roots at higher frequency at $Q = 10$, and $Q = 50$.

Figure 6(b) shows the exact neutral stability boundary determined from figure 6(a) compared against the interpolated (f, Q) neutral stability boundary given by Erpenbeck (1964) for $\gamma = 1.2$, $E = 50$. The ends of the error bars shown at fixed Q indicate the points at which Erpenbeck calculated the number of zeros of the

denominator of the transform function and made a determination of instability (to the left) or stability (to the right). The solid line is a reproduction of his hand-drawn interpolation shown in his original figure. Despite possible discrepancies due to Erpenbeck's indeterminant numerical resolution, we find that our curves lie within Erpenbeck's indicated error bars.

Figure 6(*c*) shows the neutral stability curves of the lowest frequency mode in a (f, Q)-plane for fixed γ and varying activation energy E. Again, the region to the left of the curve (towards $f = 1$) corresponds to parameter regimes of instability. The general trend that is observed is that increasing the overdrive factor for a given explosive suppresses the inherent instabilities of the flow. Also as the activation energy is increased, the region of (f, Q) parameter space that corresponds to instability increases.

Figure 7 shows the neutral stability curves corresponding to CJ detonations in a heat release–activation energy parameter plane for fixed γ, consistent with the trends shown in figure 6. The neutral stability boundary is determined by the lowest frequency mode. These curves have not been presented before and it shows that for the CJ case if the activation energy is sufficiently low, unstable modes are not present, regardless of Q.

Figure 8 shows the previously unknown dependence of one-dimensional stability on the equation of state through variations in the polytropic exponent γ. Our calculations indicate that each frequency defines a neutral stability curve that is double-valued in γ for a range of f. For fixed γ, there is a range of f for instability. For γ sufficiently large, instability is suppressed. Our partial results indicate that the neutral stability curves at higher frequencies cross at higher values of f. Whether or not there is a minimum value of γ, for all f, for stability, was left unresolved as it became difficult and expensive to compute with values of γ close to 1.

6.3. *The unstable spectrum, variation with the activation energy and the square wave limit*

The migration of the discrete spectrum as the activation energy varies is of particular interest. For large activation energy, the detonation structure connects a nearly inert induction zone to a nearly inert equilibrium zone by an R–H, discontinuity, dubbed the 'fire' by Fickett. This structure is known as the square wave. The location of the reaction zone is determined by the induction time of the reactants passing through the lead shock. Because of the simplicity of the piecewise constant structure, the square wave lies at the heart of the wave-interaction instability mechanism that was proposed by McVey & Toong (1971) and Alpert & Toong (1972). Also the large activation energy limit has been used in the previous analytical works and derives the square wave structure in a rigorous limit.

Figures 9(*a*)–9(*c*) show the results of varying the activation energy and the movement of roots in the first quadrant of the complex α-plane for the parameters $\gamma = 1.2$, $Q = 10$, $f = 2$. These figures differ only in that the scaling used to plot the results are different. The different timescales used have their origin in the characteristic times defined by the properties of the explosive and the steady solution; namely an inverse reaction time defined by the explosive independent of the steady solution $\tilde{k}$ corresponding to $\tilde{\alpha}/\tilde{k}$, the inverse reaction time at the steady shock corresponding to α and the inverse reaction time at the end of the reaction zone corresponding to $\alpha/(-r_{,\lambda}^{\infty})$.

Figure 9(*a*) plots $\alpha_i/(-r_{,\lambda}^{\infty})$ versus $\alpha_r/(-r_{,\lambda}^{\infty})$, which is how the complex growth rate naturally appears in the radiation condition and scales the complex, dimensional

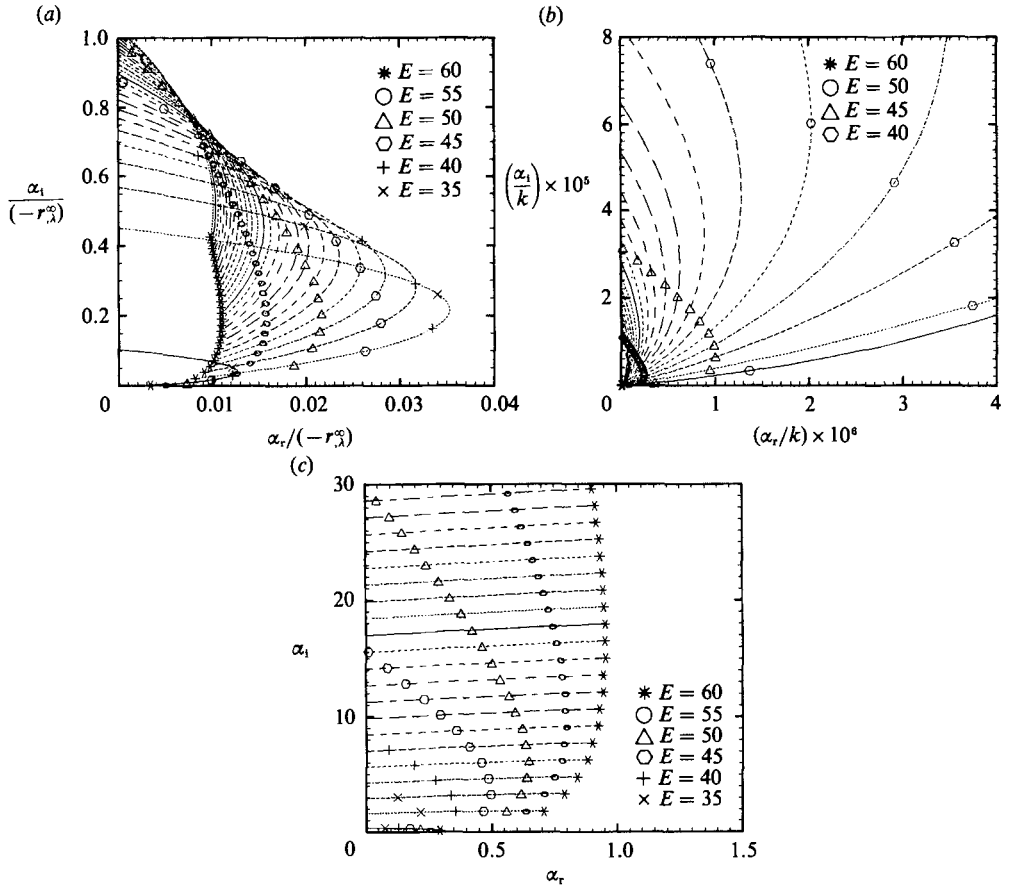

FIGURE 9. (*a*) The migration of multiple roots in the complex plane $(-\alpha_r/r^\infty_{,\lambda})$, $(-\alpha_i/r^\infty_{,\lambda})$ as E is varied. $\gamma = 1.2$, $Q = 10$ and $f = 2$, $N = 2000$. Each migration curve shown consists of approximately 200 roots. No branches lie below the lowest solid curve. Other branches above the uppermost exist for higher activation energy but are not shown. (*b*) Migration of multiple roots in the complex plane $(\tilde{\alpha}_i/\tilde{k}, \tilde{\alpha}_r/\tilde{k})$ as E is varied. $\gamma = 1.2$, $Q = 10$, $f = 2$. (*c*) Migration of multiple roots in the complex plane (α_i, α_r) as E is varied. $\gamma = 1.2$, $Q = 10$, $f = 2$.

growth rate by the inverse reaction time at the end of the reaction zone. Our calculations found these ratios directly as the roots and we found that their use effectively scaled the state dependence as E was increased, making our calculation numerically well-conditioned. The region of the search was defined by $\alpha_r/(-r^\infty_{,\lambda}) \in [0, 0.04]$ and $\alpha_i/(-r^\infty_{,\lambda}) \in [0, 1.0]$.

For the activation energy $E = 35$, a total of 3 unstable roots were found, which represents all of the unstable modes. As the activation energy was increased, more unstable roots appeared in our search window. As the activation energy was increased further, even more unstable roots appeared. It became computationally prohibitive to determine all of the high-frequency roots in our search window for the higher activation energies and we limited our computations. For example, for $E = 35$, the number of unstable roots is 3, for $E = 40$, 6, for $E = 45$, 12, for $E = 50$, 21 and for $E = 60$, the number is greater than 50! Our results suggest that as the activation energy is increased even further than we have shown, additional high-frequency instabilities appear. We speculate that the number of unstable roots

increases indefinitely with increasing activation energy. Indeed this feature alone shows how pathological the large activation energy instability is and suggests that tremendous care is needed in nonlinear numerical simulations as a direct consequence. This finding also confirms some aspects of previous work on the spectrum of the square wave detonation, which we will return to.

While figure 9(*a*) demonstrates the computational efficacy of this scaling, the physical interpretation of the behaviour of the discrete unstable spectrum is not transparent as E becomes larger. Figure 9(*b*) shows the same results where the frequencies are scaled by the inverse timescale $\tilde{k}$, which is completely independent of the dimensional activation energy. A striking conclusion from this figure is that at larger activation energies, the unstable spectrum, growth rates and frequencies decrease exponentially. A physical reason for this is that as the activation energy increases, the induction time and corresponding induction length increase exponentially. Consequently any instability mechanism that is associated with the round trip traversal of acoustic waves between the shock and reaction zone takes an infinitely long time to occur. For $E = \infty$, the shocked material does not react and the system has the stability of the step shock, which in this case is neutrally stable.

Figure 9(*c*) shows the spectral results using $\tilde{t}_c$ (which is proportional to the induction time for large activation energy) as the scaling and yields another interesting physical interpretation. Note that once an unstable mode is present, its growth rate changes with increasing activation energy, but its frequency is nearly constant. Also the change in frequency plotted versus mode number was found to be nearly constant as the activation energy is increased at increments of $\tilde{\alpha}\tilde{t}_c$ of about 1.4. Thus our results suggest that the fundamental period of instability is proportional to the induction time and shows clearly that the unstable higher-frequency modes are essentially integer multiples of the lowest frequency, as might be expected. This theoretical observation is consistent with the experimental correlations of McVey & Toong and Alpert & Toong.

McVey & Toong and Alpert & Toong gave a physical interpretation of the longitudinal instability based on the implicit assumption of the square wave structure. They suggested that the instability mechanism is maintained by a cycle where a compressive acoustic disturbance reflects off the shock to create a thermal disturbance which is then carried on particle lines which shortens the induction time for reaction, causing a rapid acceleration of the fire. The accelerating fire creates compressive waves that propagate both towards the shock and into the burnt region. While the forward pulse is the origin of the original compressive wave that starts the cycle, the back facing pulse becomes a relatively strong rarefaction that later serves to weaken the leading shock. The fire continues accelerating towards the shock until such time that the rarefaction from the previous cycle weakens the shock and increases the induction time. One important conclusion of their work is that this mechanism of instability must occur on the scale of the induction time. Our results shown in figure 9(*c*) demonstrate this correlation convincingly for reasonably large activation energy and from the point of view of the linear acoustics of stability theory, confirm a reflection mechanism.

Our numerical results seem consistent with some aspects of the previous analyses of the square wave detonation. Analyses of the square wave model by Erpenbeck (1963), Fickett (1985) and Buckmaster & Nevis (1988), all share the common pathology in the description of the unstable spectrum in that the most unstable roots occur at high (infinite) frequency. Our results show, at least for moderate activation energy, that the spectrum has a maximum growth rate and then stabilizes at higher

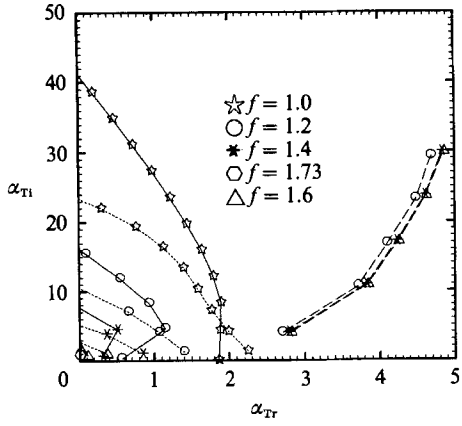

FIGURE 10. Comparison of the unstable spectra calculated by Abouseif & Toong, Buckmaster & Nevis and the present work for $\gamma = 1.2$, $E = Q = 50$ and $f = 1.0$, 1.2, 1.4 and 1.6. The results are shown in units of half-reaction time as defined by Abouseif & Toong. ——, results of this paper. — — —, Buckmaster & Nevis. – –, Abouseif & Toong.

frequency. This result was speculated on by Buckmaster & Nevis, suggesting that the square wave results are incomplete. Our numerical results also show that, at the highest activation energies that we computed with (e.g. $E = 60$), at low frequencies, the growth rates of the spectrum grow with increasing frequency. At higher frequencies (even for $E = 60$) the growth rates decrease with increasing frequencies.

It is likely that the square wave analyses are properly identifying the lower-frequency portion of the spectrum but not the higher-frequency portion. The theoretical reason for this deficiency is clear; all these analyses have not considered the complete structure of the reaction zone. Very high-frequency disturbances are likely to originate from the passage of the acoustic waves through the extremely thin reaction (fire) zone. In contrast, our stability formulation is in terms of the reaction coordinate and the entire structure is treated with no approximations.

The studies by Abouseif & Toong and Buckmaster & Nevis give explicit results for the spectrum such that a comparison can be made with our results. This is shown in figure 10 and table 1 for $\gamma = 1.2$, $Q = E = 50$, with $f = 1.0$, 1.2, 1.4 and 1.6. All researchers used slightly different dimensional scalings. Abouseif & Toong define the timescale as the steady half-reaction time, $\tilde{t}_{\frac{1}{2}}$ and the lengthscale by $\tilde{c}_0 \tilde{t}_{\frac{1}{2}}$. Buckmaster & Nevis define the lengthscale by an asymptotic expression for the induction length $\tilde{L}$ and the timescale by $\tilde{L}/\tilde{c}_s$. Likewise we have defined the lengthscale by the steady half-reaction length $\tilde{l}_c$ (which becomes commensurate with $\tilde{L}$ as $E \to \infty$) and the timescale as $\tilde{l}_c/\tilde{c}_s$. Appendix B gives the formulae for conversion of scales.

Abouseif & Toong gave an approximate but non-rigorous calculation for the spectrum based on activation-energy asymptotics but applied for finite activation energies. Quoting Buckmaster & Nevis, 'But in addition, the approximations that are at the heart of the calculations of Abouseif and Toong, raise serious doubts about the accuracy of their results. It is sufficient to consider one of the approximations. Instead of solving the exact linearized equations with coefficients defined by the exact steady solution, they linearize all nonchemical terms about the steady postshock state. Thus all nonchemical terms have constant coefficients.... These cannot be valid within the fire or the burnt gas and it is difficult to assess the effect of their approximations on the final results. Clearly there is a need for numerical calculation without extrarational approximation.'

		Lee & Stewart ($N = 2000$)		Nonlinear simulation (Abouseif & Toong and Fickett & Wood)	Abouseif & Toong		Buckmaster & Nevis	
f	n	α_{Tr}	α_{Ti}	α_{Ti}	α_{Tr}	α_{Ti}	α_{Tr}	α_{Ti}
1	1	1.857	0.000	0.314	2.24	1.31	—	—
	2	1.879	4.372	4.2	1.99	4.16	—	—
	3	1.888	8.333	—	1.76	7.2	—	—
	4	1.785	12.16	—	1.58	10.28	—	—
	5	1.634	15.96	—	1.39	13.35	—	—
	6	1.434	19.74	—	1.12	16.40	—	—
	7	1.214	23.53	—	0.76	19.35	—	—
	8	0.973	27.31	—	—	—	—	—
	9	0.721	31.09	—	—	—	—	—
	10	0.459	34.87	—	—	—	—	—
	11	0.189	38.65	—	—	—	—	—
	12	−0.088	42.43	—	—	—	—	—
1.2	1	0.569	0.300	0.45	1.40	1.21	2.71	3.95
	2	1.148	4.547	4.2	1.07	4.02	3.72	10.6
	3	0.933	8.234	—	0.66	7.00	4.11	16.8
	4	0.550	11.84	—	−0.20	11.64	4.48	23.2
	5	0.095	15.44	—	—	—	4.69	29.3
	6	−0.400	19.03	—	—	—	—	—
1.4	1	0.313	0.664	0.785	0.84	1.04	2.80	4.03
	2	0.504	4.484	4.2	0.36	3.82	3.83	10.9
	3	−0.041	7.913	—	−0.38	6.52	4.23	17.2
	4	−0.763	11.29	—	—	—	4.61	23.7
	5	−1.540	14.64	—	—	—	4.84	30.0
1.6	1	0.112	0.789	0.785	0.372	1.00	2.82	4.03
	2	−0.076	4.314	—	−0.132	3.4	3.85	10.9
	3	−0.952	7.472	—	−0.646	6.4	4.25	17.2
	4	−1.966	10.58	—	—	—	4.62	23.7
	5	−2.790	13.48	—	—	—	4.86	30.0
1.731	1	0.000	0.825	—	—	—	—	—

TABLE 1. Comparison of the unstable spectrum between Lee & Stewart, Abouseif & Toong, Buckmaster & Nevis, and the simulations of Fickett & Wood. $\gamma = 1.2$, $Q = 50$, $E = 50$. n is the mode number. α_T is the complex frequency scaled with the half-reaction time.

Abouseif & Toong's approximate spectrum does not agree with the exact result. Their growth rates and higher frequencies are overpredicted. Contrary to our results they show the maximum growth rate always occurs at the fundamental (lowest) frequency. Their results are surely affected by their ad hoc approximations and the truncation of terms in their stability calculations.

The results of Buckmaster & Nevis are asymptotically derived in the limit of large activation energy and their leading-order estimates of the frequencies and growth rates are shown for finite activation energy in figure 10 for comparison. While only 5 eigenvalues are given, they, in principle, calculate an infinite number. The quantitative comparison of their results with ours and Abouseif & Toong's results is poor for $E = 50$. And they show an opposite trend of increasing instability as the overdrive factor, f, is increased. However it is not clear that $E = 50$ is large enough

to expect their results to agree quantitatively, although on a physical basis $E = 50$ is a large activation energy. Also, for $Q = E = 50$ the exact steady state structure does not look like a square wave. There is theoretical reason to suspect their result which is given below.

In their analysis they treat only the induction zone with slight reaction. The acoustic equations in the induction zone are solved subject to the linearized shock conditions and a homogeneous boundary condition that the temperature perturbation is zero at the end of the induction zone. The rationale for this last condition is to ensure a regular solution of the perturbations as the end of the induction zone is approached. In doing this they derive the spectral results shown.

They do not attempt to solve for the complete eigenfunction through the induction zone, fire, to the end of the equilibrium zone where the radiation condition (4.26)–(4.27) must apply. Stewart & Kapila have made some preliminary calculations on the large activation energy limit, with the complete formulation of the singular eigenvalue problem given here. These calculations show the eigenfunctions to obey the same equations as Buckmaster & Nevis in the induction zone, however, in order to match with the solutions in the fire zone, a stronger condition on the eigenfunctions must hold at the end of the induction zone; namely that both the pressure and density perturbations vanish. This stronger condition is consistent with the vanishing of the temperature as Buckmaster & Nevis assumed, but it means that their stability problem, confined only to the induction zone would be overdetermined. Of course this stronger condition presents no difficulty when properly viewed as a statement about the structure of the eigenfunctions and as a matching condition for the continuation of the eigenfunctions through the reaction zone.

It may turn out that the Buckmaster & Nevis estimate of the spectrum for $E \to \infty$ is correct and describes only the lower-frequency portion of the spectrum. If this is the case, then tremendously large values of E, larger than used in this study, are required to make a quantitative comparison.

A fair amount of effort has been expended in comparison of results of linear stability to the isolated case of $\gamma = 1.2$, $Q = E = 50$ and $f = 1.6$. The value of $f = 1.6$ is extremely close to the neutral stability boundary. Indeed our calculations show that the neutrally stable value of f is 1.731 with $\tilde{\alpha}_i \tilde{t}_{\frac{1}{2}} = 0.825$ corresponding to an oscillation period of the fundamental mode of 7.616, measured in steady half-reaction times. Large amplitude simulations of Fickett & Wood and later ones by Abouseif & Toong have a low-frequency oscillation of about 8 half-reaction times. Close inspection of these simulations shows variations of the period measured between peaks of the pressure oscillation to be approximately 10%. Abouseif & Toong report that they found that both 'the amplification rate and the amplitude of oscillation were slightly dependent on the step size used in numerical calculation'. Unfortunately no details are given. During the revision of this paper, the results of new numerical simulations using front tracking of the lead shock and the piecewise parabolic method (PPM) were carried out by Bourlioux, Majda & Roytburd (1989) which found the transition to instability at $f = 1.731$. Indeed they used the method and formulation of this paper to calculate the growth rates, frequencies and eigenfunctions and made comparisons with the nonlinear simulations and found excellent agreement.

In summary, our lowest-frequency linear stability results are in rough agreement with those observed in the nonlinear simulation reported by Fickett & Wood and Abouseif & Toong at large disturbance amplitudes and in exact agreement with the recent work near the stability boundary done by Bourlioux & Majda.

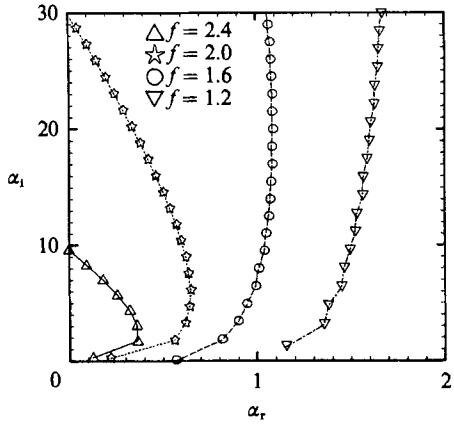

FIGURE 11. The unstable spectra for $\gamma = 1.2$, $Q = 50$, $E = 10$ and for $f = 1.2$, 1.6, 2.0 and 2.4.

6.4. *Other results*

A general study of the migration of the unstable spectrum for large but finite activation energy (as well as for other parameters) is computationally intensive because of the stiff nature of the governing equations. For example, figure 9 required approximately 5 hours of CPU time on a CRAY XMP-48 computer to generate it. All of the roots were not determined at the higher frequencies owing to our computational restrictions. Thus a study at truly large but finite activation energy is still incomplete and likely to be difficult. For example, we have made no attempt to study methodically the frequency of the most unstable growth rate in parameter space. The interesting question of how the spectrum varies with the other parameters such as γ, Q and f is as yet incomplete. Completion may require alternative numerical methods to be applied to this problem. At the time of this writing we are aware of an independent effort to examine this difficult question at large but finite activation energies by Lainé-Schmidt and coworkers by means of collocation schemes (private communication).

Results of another migration study are shown in figure 11, for $\gamma = 1.2$, $Q = 10$, $E = 50$ with $f = 1.2$, 1.6, 2.0 and 2.4, which complements figure 10. The results show that as the overdrive factor is increased, stability is achieved and the most unstable modes are at the lowest frequencies. Thus the effect of changing E is opposite to changing f, since as E is lowered, instability is suppressed and the lower-frequency modes tend to be the most unstable.

Finally, as an experiment, we decided to require that the velocity perturbation be zero at the end of the steady reaction zone, $u' = 0$, replacing the radiation condition (4.26)–(4.27), to test the sensitivity of our computed stability results to the rear boundary condition. This condition mimics a constant-velocity piston supporting the flow. Comparison of the neutral stability curves obtained for the radiation condition and the zero perturbation particle velocity condition is shown in a portion of the (f, Q)-plane for fixed $\gamma = 1.2$, $E = 50$ in figure 12 for the lowest-frequency mode. In the range shown there is at most a 10% difference in the results.

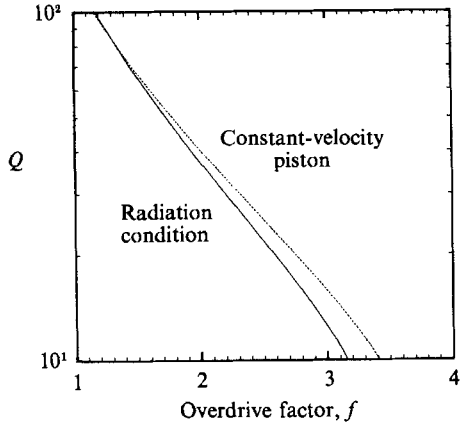

FIGURE 12. Comparison of the neutral stability curves obtained for the radiation condition and a zero perturbation particle velocity applied at the piston. The results are shown in a (Q,f)-plane for fixed $\gamma = 1.2$, $E = 50$. In the range shown there is at most a 10% difference in the results.

7. Future work

We have presented a direct normal mode approach to the detonation stability problem which greatly simplifies the formulation and the calculation of linear instability of detonation. This method directly calculates the dispersion relation and unstable eigenfunctions. In this paper we have limited the discussion to one-dimensional instability. Multidimensional instability is treated by exactly the same methodology since consideration of transverse disturbances only introduces an additional parameter ϵ (say) which corresponds to the square root of the sum of the squares of the transverse wavenumbers. We will report on these results in a sequel.

Our method may be able to treat the stability of more complex systems with regard to changes in the equation of state and the kinetics of the reaction driving the detonation. The normal mode approach and the use of the shooting method or its equivalent is, in principal, capable of being generalized to equations of state and kinetic schemes of the form

$$\dot{e} = e(p, \nu, \lambda_1, \lambda_2, \lambda_3 \ldots \lambda_n), \quad \mathrm{D}\lambda_i/\mathrm{D}T = r_i(p, \nu, \lambda_1, \lambda_2, \lambda_3 \ldots \lambda_n) \quad (i = 1, \ldots, N). \tag{7.1}$$

In particular, the state vector $\boldsymbol{z}$ is increased in length by $N-1$ with the addition of equations (7.1*b*). However the general question as to the nature of the rear boundary condition in the equilibrium zone must be resolved for these general schemes.

Finally, we point out that even though our scheme is direct and easy to implement, complete investigation of the various regions of parameter space is computationally intensive. Any equivalent or more efficient numerical method for computation of detonation should be considered a valuable contribution and such approaches are needed to further explore the parameter regimes of instability.

The authors would like to acknowledge the indispensable encouragement and support of our colleagues at M-division at Los Alamos National Laboratory. H. I. L. acknowledges computing support from the Department of Aeronautics and Astronautics at the University of Illinois and encouragement from Professors Buckmaster and Hilton. This paper was greatly improved during the revision by

suggestions and comments of J. Bdzil, W. Fickett, J. Erpenbeck, R. Klein and the referees. This work has been supported through a contract with Los Alamos National Laboratory, DOE-LANL-9XG8-3931-P1 and the National Center for Supercomputing Applications.

Appendix A. Definition of $\boldsymbol{L}$ and $\boldsymbol{L}_{\mathrm{CJ}}$

The quantities S_1, S_2 and S_3 are defined as the first three terms on the diagonal of the scaling matrix $\boldsymbol{S}$. Thus we find that

$$\boldsymbol{L} \equiv -(\alpha \hat{\boldsymbol{F}}^* + \hat{\boldsymbol{G}}^*)$$

$$= \eta_\infty^{-1} \begin{bmatrix} \eta_\infty(\alpha/r^\infty_{,\lambda}) & -(\alpha/r^\infty_{,\lambda})(S_2/S_1)M^2_\infty/M_s & (\alpha/r^\infty_{,\lambda})(S_3/S_1)M^2_\infty/(M_s^2\gamma) \\ 0 & -(\alpha/r^\infty_{,\lambda})M^2_\infty & (\alpha/r^\infty_{,\lambda})(S_3/S_2)M^2_\infty/(M_s\gamma) \\ 0 & (\alpha/r^\infty_{,\lambda})(S_2/S_3)\gamma M_s & -(\alpha/r^\infty_{,\lambda})M^2_\infty \\ 0 & 0 & 0 \end{bmatrix}$$

$$\begin{bmatrix} -(\gamma-1)\beta M^2_\infty/(\gamma M_s^2 \nu_\infty S_1) \\ -(\gamma-1)\beta M^2_\infty/(\gamma M_s \nu_\infty S_2) \\ (\gamma-1)\beta M^2_\infty/(\nu_\infty S_3) \\ \eta_\infty[(\alpha/r^\infty_{,\lambda})-1] \end{bmatrix}. \quad \text{(A 1)}$$

$$\boldsymbol{L}_{\mathrm{CJ}} \equiv -(\alpha \hat{\boldsymbol{F}}^*_{\mathrm{CJ}} + \hat{\boldsymbol{G}}^*_{\mathrm{CJ}})$$

$$= a(1-M_s^2)^{-1} \begin{bmatrix} 0 & -(\alpha/r^\infty_{,\lambda})(S_2/S_1)/M_s & (\alpha/r^\infty_{,\lambda})(S_3/S_1)/(M_s^2\gamma) \\ 0 & -(\alpha/r^\infty_{,\lambda}) & (\alpha/r^\infty_{,\lambda})(S_3/S_2)/(M_s\gamma) \\ 0 & (\alpha/r^\infty_{,\lambda})(S_2/S_3)\gamma M_s & -(\alpha/r^\infty_{,\lambda}) \\ 0 & 0 & 0 \end{bmatrix}$$

$$\begin{bmatrix} -(\gamma-1)\beta/(\gamma M_s^2 \nu_\infty S_1) \\ -(\gamma-1)\beta/(\gamma M_s \nu_\infty S_2) \\ (\gamma-1)\beta/(\nu_\infty S_3) \\ 0 \end{bmatrix}. \quad \text{(A 2)}$$

Appendix B. Conversion of timescales

Using the definitions of the timescales and lengthscales given in Buckmaster & Nevis (1988) and Abouseif & Toong (1982), the following conversion formulae are derived. The subscript B, refers to Buckmaster & Nevis. The subscript T refers to Abouseif & Toong.

$$\alpha_{\mathrm{T}}/\alpha = \frac{\int_0^{\frac{1}{2}} (1-s)^{-1} \exp(\theta/(p^*\nu^*))\,\mathrm{d}s}{\int_0^{\frac{1}{2}} u^*(1-s)^{-1} \exp(\theta/(p^*\nu^*))\,\mathrm{d}s}, \quad \text{(B 1)}$$

$$\alpha_{\mathrm{T}}/\alpha_{\mathrm{B}} = \frac{(\gamma-1)(M_s^2-1/\gamma)}{M_s(M_s^2-1)}\theta\beta \int_0^{\frac{1}{2}} (1-s)^{-1} \exp(\theta/(p^*\nu^*)-\theta)\,\mathrm{d}s. \quad \text{(B 2)}$$

REFERENCES

ABOUSEIF, G. & TOONG, T. Y. 1982 Theory of unstable one-dimensional detonations. *Combust. Flame* **45**, 67–94.

ALPERT, R. L. & TOONG, T. Y. 1972 Periodicity in exothermic hypersonic flows about blunt projectiles. *Acta Astron.* **17**, 538–560.

BDZIL, J. B. & STEWART, D. S. 1986 Time-dependent two-dimensional detonation : the interaction of edge rarefactions with finite-length reaction zones. *J. Fluid Mech.* **171**, 1–26.

BOURLIOUX, A., MAJDA, A. J. & ROYTBURD, V. 1989 Theoretical and numerical structure for unstable one-dimensional detonation. Preprint.

BUCKMASTER, J. D. & LUDFORD, G. S. S. 1988 The effect of structure on the stability of detonations I. Role of the induction zone. In *Proc. Twenty-First Symp. (Intl) on Combustion*, pp. 1669–1675. The Combustion Institute, Pittsburgh, PA.

BUCKMASTER, J. D. & NEVIS, J. 1988 One-dimensional detonation stability – The spectrum for infinite activation energy. *Phys. Fluids* **31**, 3571–3575.

ERPENBECK, J. J. 1962 Stability of steady-state equilibrium detonations. *Phys. Fluids* **5**, 604–614.

ERPENBECK, J. J. 1963 Structure and stability of the square-wave detonation. In *Ninth Symp. (Intl) on Combustion*, pp. 442–453. Academic.

ERPENBECK, J. J. 1964 Stability of idealized one-reaction detonations. *Phys. Fluids* **7**, 684–696.

FICKETT, W. 1985 Stability of the square wave detonation in a model system. *Physica* **16D**, 358–370.

FICKETT, W. & DAVIS, W. C. 1979 *Detonation*. University of California Press.

FICKETT, W., JACOBSON, J. D. & WOOD, W. W. 1970 The method of characteristics for one-dimensional flow with chemical reaction. *Los Alamos Scientific Laboratory Rep.* LA-4269.

FICKETT, W. & WOOD, W. W. 1966 Flow calculations for pulsating one-dimensional detonations. *Phys. Fluids* **9**, 903–916.

MCVEY, J. B. & TOONG, T. Y. 1971 Mechanism of instabilities in exothermic blunt-body flows. *Combust. Sci. Tech.* **3**, 63–76.

MAJDA, A. & ROSALES, R. 1983 A theory for spontaneous Mach stem formation in reacting shock front, I. The basic perturbation analysis. *SIAM J. Appl. Maths* **43**, 1310–1334.

SHEPHERD, J. E. 1986 Chemical kinetics of hydrogen–air–diluent detonations. *Prog. Aeronaut. Astronaut.* **106**, 263–293.

STEWART, D. S. & BDZIL, J. B. 1988*a* The shock dynamics of stable multidimensional detonation. *Combust. Flame* **72**, 311–323.

STEWART, D. S. & BDZIL, J. B. 1988*b* A lecture on detonation shock dynamics. In *Mathematical Modelling in Combustion Science* (ed. J. B. Buckmaster & T. Takeno). Springer.